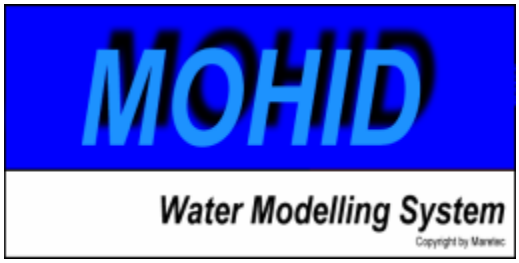

Test case application

Ocean Model for CSO Impact on Receiving Waters

DATE :	**23/NOV/2005**	
Authors:	**Coordination**	**Ramiro Neves (IST)**
	Team	**Paulo Leitão (Hidromod)** **Luís Fernandes (IST)** **Frank Braunschweig (IST)**
Language:	**English**	

INDEX

1. Executive summary 6

2. Introduction 8

3. Test Case Description 10

4. Model Setup as Requested 12

4.1.1 Results 13

4.1.2 About the Runs 19

5. Alternative Hydrodynamic Model Setup 20

5.1 Cyclic Open-Boundary Condition 20

5.1.1 Model setup 20

5.1.2 Results 21

5.2 3D Simulations 24

5.2.1 Model setup 24

5.2.2 Results 24

6. Biogeochemical Simulations 32

6.1 Model setup 33

6.1.1 Results 35

6.1.2 About the Runs 40

7. Conclusions 41

8. References 42

FIGURES INDEX

Figure 1 - Test Case — View from above. 10

Figure 2 - Test Case — Vertical view of A-A' Cut. 11

Figure 3 – Domain bathymetry 12

Figure 4 – Test-case - Velocity field after 5 days of simulation (velocity arrows plotted every 6 grid cells) 15

Figure 5 – Test-case – Free surface elevation and velocity field after 5 days of simulation (velocity arrows plotted every 6 grid cells) 15

Figure 6 – Detail of flow field around the obstacle after 5 days of simulation 16

Figure 7 - Evolution sea level in the selected locations 16

Figure 8 - Evolution East-West velocities in the monitoring stations 17

Figure 9 - Evolution of South-North velocities in the monitoring stations 17

Figure 10 - Evolution of contaminant concentrations in the selected locations 18

Figure 11 – Contaminant concentration field after 5 days of simulation. 19

Figure 12 – a) level 1 bathymetry; b) level 1 bathymetry overlapped by level 2 bathymetry. 21

Figure 13 – Velocity field of level 1 overlap by the level 2 solution. Vectors are plotted every 6 cells. 22

Figure 14 – Detail of the circulation immediately downstream of the obstacle. Vectors are plotted every 3 cells. Vectors are only plotted for intensities lower than 10 cm/s... 22

Figure 15 – Contaminant plume with a first order decay (T90 = 5 hours) 23

Figure 16 – Surface layer velocity field after a 5 days run. Vectors are represented in every cell 25

Figure 17 - Bottom layer velocity field after a 5 day run. Vectors are represented in every cell 25

Figure 18 – Surface layer salinity and velocity field for the level 2 domain 26

Figure 19 – Bottom layer salinity and velocity field for the level 2 domain. 26

Figure 20 – Surface layer velocity field for the 3D case (vectors in black) overlapped by the 2D case (vectors in red) 27

Figure 21 - Bottom layer velocity field for the 3D case (vectors in black) overlapped by the 2D case (vectors in red)..... 28

Figure 22 – Surface layer contaminant concentration (eulerian results) and velocity field. 29

Figure 23 – Surface layer contaminant concentration (lagrangian results) and velocity field. 30

Figure 24 – Bottom layer contaminant concentration (eulerian results) and velocity field. 30

Figure 25 – Bottom layer contaminant concentration (lagrangian results) and velocity field. 31

Figure 26 – Velocity field and in red are presented all the tracers position (their number is of the order of 90.000)..... 31

Figure 27 – MOHID Water Quality Module: Main processes involving phytoplankton. 32

Figure 28 – Phytoplankton concentration evolution in the defined stations. Simulations started at 12h00 and consequently “1 day” simulation is also at noon. Having this in mind it is clear that maximum concentration is reached by the end of the day light..... 36

Figure 29 – Surface phytoplankton concentration after 6 hours of simulation..... 37

Figure 30 - Surface phytoplankton concentration after 24 hours of simulation..... 37

Figure 31 - Surface phytoplankton concentration after 2 days and 6 hours of simulation 38

Figure 32 - Surface phytoplankton concentration after 2 days and 18 hours of simulation..... 38

Figure 33 - Surface ammonia concentration after 2 days and 6 hours of simulation.... 39

Figure 34 - Surface nitrate concentration after 2 days and 6 hours of simulation 39

TABLES INDEX

Table 1 – Summary of parameters for the test-case simulations 11

Table 2 – Discharge and ambient parameters concentrations 34

Table 3 – Meteorological conditions used in the biogeochemical simulations..... 34

Table 4 – Fine sediment transport parameters..... 35

1. Executive summary

This report was prepared as part of the answer of MOHID developers group to the questionnaire received from Clabsa SA. In that questionnaire the group was asked to run the hydrodynamic and advection-diffusion transport model in a test case, for which all the parameters and boundary conditions were specified.

MOHID developers group has interpreted the questionnaire as a way to know more about the model and the test case as an objective quantification of the model capacity. Having this in mind, it was decided to complement this test with some extra simulations to illustrate the ability of the model to deal with different boundary conditions, but also for putting into evidence the importance of that capacity in practical applications.

The report includes hydrodynamic results as demanded in the questionnaire, but also (1a) hydrodynamic results obtained using alternative boundary conditions (combination of a cyclic boundary condition and a radiative boundary condition using nested models) and (1b) hydrodynamic results using a 3D formulation and (2) results of a water quality model based on the 3D simulations. A comparison of a lagrangian and a eulerian approach is also included.

The results of the hydrodynamic model have shown that the solution is highly dependent on the boundary condition used, putting into evidence that on one hand (1) it is very important to specify exactly the conditions of the simulation (as was done in the questionnaire), and on the other hand (2) for real situations it is important to have a model that is able to use the most adequate boundary conditions.

Using the boundary conditions specified in the questionnaire, the flow is controlled by inertia and converges to the southern corner next to the eastern boundary. Behind the obstacle there is a region of low velocity, but no recirculation is identified. Using a cyclic/radiative boundary condition, emulating an infinite rectilinear coastline where an obstacle is placed, velocities are higher and the general flow is controlled by longitudinal equilibrium between wind drag and bottom friction and transversally by equilibrium between coriolis and pressure forces.

The results of the 3D simulations put into evidence the importance of the vertical processes in flows where density plumes are submitted to a surface wind forcing. In the case studied, surface velocity increased by about 25% and the recycling zone in the shadow of the obstacle does not reach the surface (because the wind is very strong).

The biogeochemical processes are not very important in this case because the residence time is of the order of 6 hours. The results showed however that they are more important in the shallower areas and in regions downstream the modelling area.

The Lagrangian simulations are not very useful in this particular case because the plume dimension is of the order of the size of the simulation domain (one half). They would however be very useful in real situations when the area of simulation must be much larger than the plume size (because of wind direction variability and for simulating the fate of the material discharged and not only the dispersion in the vicinity of the diffuser).

For obtaining results quickly and for simplifying code maintenance/expansion a model, likewise MOHID, must (1) have a well organized and clear code, (2) deal with boundary conditions on a systematic way, (3) have a robust input module (for avoiding input data errors) and (4) be equipped with a good post processing tool. Thus, the sum of pre-processing, execution and post-processing times is less important then the time occupied in scenarios definition and results analysis and interpretation, when the aim is to produce high quality simulations.

2. Introduction

This report describes the results of MOHID Water Modelling System (http://www.mohid.com) for the test case application proposed in the questionnaire entitled “Ocean Model for CSO Impact on Receiving Waters”. The simulations proposed in the questionnaire were complemented with two additional hydrodynamic scenarios: (i) Radiative Open-Boundary and (ii) Three-Dimensional simulation. Also the consideration of biogeochemical processes (nitrogen cycle) complements this report further down.

MOHID is an integrated modelling tool developed at Instituto Superior Técnico (Engineering School of the Technical University of Lisbon) under the supervision of Prof. Ramiro Neves, in the research centre Maretec. MOHID has two major components: (a) MOHID Water simulates the hydrodynamics and biogeochemical processes in free-surface water bodies and (b) MOHID Land is being developed for simulating flow in river catchments. MOHID is designed using an object-oriented programming philosophy, which enables the straightforward integration of several different environmental processes.

MOHID is being developed since the middle eighties by several generations of post-graduation students, having originated 11 PhD Thesis and more than 20 MSc Thesis. Presently the research group includes 2 Professors (Ramiro Neves and Aires dos Santos), 13 PhD students and 7 master students. Hidromod Lda, is a spin-off company created by former PhD students in 1992 and has always worked in close collaboration with Maretec. Presently Hidromod has 6 people, including 4 PhD’s. The results presented in this report were produced by researchers from IST (Ramiro Neves, Luis Fernandes and Frank Braunschweig) and by Paulo Leitão from Hidromod.

In the chapter entitled “Model Setup as Requested”, are presented the results for the test-case using the spatial-step and Open Boundary Conditions (OBC) requested in the questionnaire. Information requested (e.g. run time) is also presented together with the description of the assumptions made.

In the chapter “Alternative Model Setup” are shown results obtained using an alternative OBC (radiative boundary condition), both in a 2D and in a 3D implementation. In the latter case a grid size of 100 meters was used. This test illustrates the ability of MOHID to deal with different OBC, but also the sensitivity of the results to the OBC and to simulate 3D effects associated to the wind and to the discharge of fresh water in the sea.

In the final chapter, results for the 3D simulation of biogeochemical processes (nitrogen cycle) are presented. Biogeochemical processes are not relevant at the scale of this test (the residence time is shorter than one day), but they can be relevant in an integrated coastal management approach at a larger spatial scale, e.g. for assessing the benefits of alternative inland treatment levels. MOHID was designed having this goal in mind.

3. Test Case Description

The test consists of analyzing contaminant dispersion past a shoreline obstacle in a schematic situation, where the flow is driven by a permanent wind parallel to the coastline. The horizontal dimensions and the obstacle are show in Figure 1 and the bottom profile in Figure 2. Figure 1 also shows the points (P1 to P4) where the solution of the model must be monitored in time.

The geometry is rectangular (10000 x 5000m^2), it is opened on three sides and a pollution source is situated 1000 m upstream of a square obstacle with dimensions 1000 x 1000 m^2. The bottom slope is uniform (1/25) as shown in Figure 2 where the cross section A-A' shown in Figure 1 is represented.

The flow is forced by a permanent and uniform wind parallel to the coastline, with velocity of 10m/s at 10m height. Initially, fluid is at rest (null velocity and elevation). The contaminant source is a constant discharge of 50 m^3/s of decaying matter with concentration of 10^6 mg/l.

As boundary conditions for open boundaries, null elevation and null velocity gradient are to be considered. Calculation mesh must be rectangular, structured and uniform, with 500 x 250 elements of 20 x 20 m^2. These conditions, together with other parameters required by the model are summarized in Table 1.

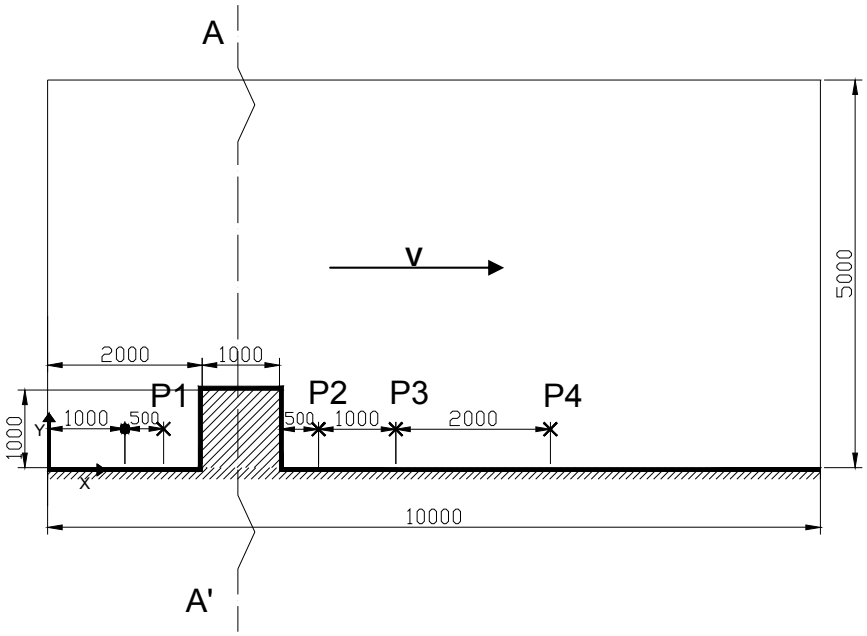

Figure 1 - Test Case — View from above.

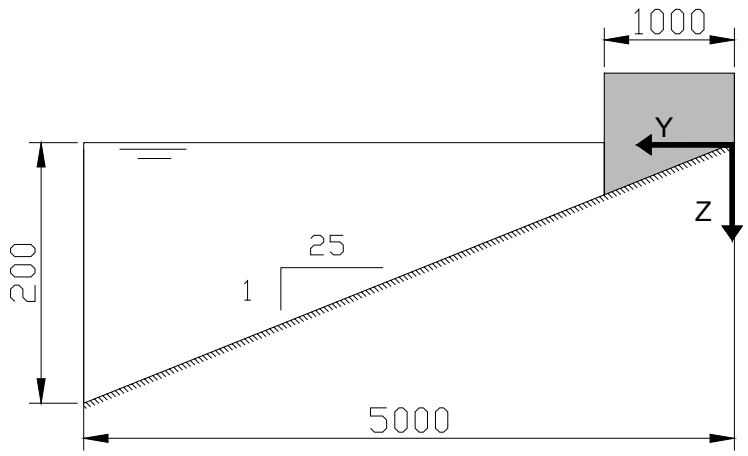

Figure 2 - Test Case — Vertical view of A-A' Cut.

Table 1 – Summary of parameters for the test-case simulations

Hydrodynamics

Δx	Mesh spacing in x direction	20 m
Δy	Mesh spacing in y direction	20 m
u_0, v_0	Initial velocities in x and y	0 m/s
η_0	Initial elevation	0 m
V	Wind velocity at 10 m	10 m/s
C_D	Wind drag coefficient	0,0025
C_F	Bottom friction coefficient	0,0025

Advection/Dispersion

C_0	Source concentration	10^6 mg/l
Q	Flow rate	50 m^3/s
K	Dispersion coefficient	3,6 m^2/s
T_{90}	Decaying time of 90% of mass	5 hours

4. Model Setup as Requested

This chapter describes the results of the model implemented using the exact conditions described in the questionnaire. Figure 3 shows the bathymetry defined in the 20m resolution grid and the position of the discharge and of the monitoring points.

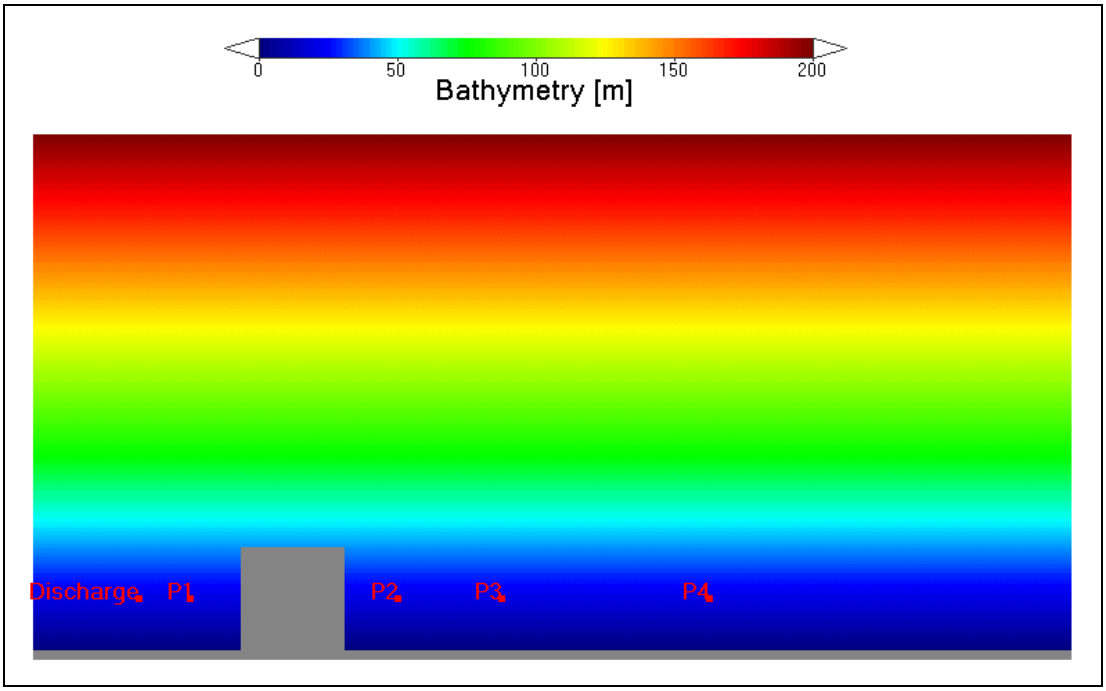

Figure 3 – Domain bathymetry

As some parameters were not defined explicitly in the benchmark terms, the following approaches were assumed:

Vertical discretization and forces involved

- The model was setup in the vertically integrated mode (2D);
- No baroclinic effects were considered;

Advection schemes

- TVD with Superbee flux limitation advection scheme was used to compute momentum and mass transport;

Coriolis force

- The domain was setup with a reference latitude and longitude of 40.5º N and 0.5º E respectively. This latitude value was used to compute the Coriolis parameter.

Boundary conditions

- No slipping condition was used both in bottom and lateral boundaries;
- Using the defined wind drag coefficient (0.0025), a constant wind shear stress in the X direction of 0.25 Pa was applied;

Contaminant transport

- An eulerian approach was followed to simulate decaying matter transport;
- The ambient concentration of the contaminant was assumed to be 0.001 mg/l;
- Due to the model being run in a vertically integrated mode, the discharge is distributed in one control volume, thus with no associated depth. The discharge was also deviated 10m southward and 10 m eastward, as the grid cells boundaries coincide with the exact discharge location; The same was assumed with points P1, P2, P3 and P4, where results time series results are analyzed.

Time step and simulation period

- A time step of 10 seconds was used. As MOHID's hydrodynamic module uses a time splitting technique and the maximum water column depth is approximately 200m with a 20m grid resolution, the maximum Courant number is around 40 in the deepest areas. This does not compromise the results because in those areas the flow is parallel to the grid and gradients are small.
- The simulation period, 5 days, was defined from 00h00 of 1st January 2005 until 00h00 of 6th January 2005 (in this case this is not relevant for computations. It's just a matter of time reference for the outputs).

4.1.1 Results

The velocity field after 5 days simulation is shown in Figure 4 and in Figure 5. The former shows the velocity (colour shows intensity) and the latter shows velocity and level (in colour). Globally one can say that (1) velocity is higher in the shallower areas, (2) maximum velocity is reached close to the south-eastern boundary (assuming north to be offshore perpendicular to the coastline) and (3) there is no clear recirculation behind the obstacle.

Higher velocities in the shallower areas are a consequence of inertia being smaller there. The maximum velocity at the south-eastern corner is a consequence of the null free surface level imposed along the open boundary and of its interaction with the Coriolis force.

When the simulation starts, wind forces the water to move eastward. This flow is deflected by Coriolis force to the southern solid boundary forcing the water level to rise there, creating a southward pressure gradient that redirects the flow to become again parallel to the coastline. This pressure gradient is destroyed at the boundary by the "zero level" imposed OBC, resulting into a reorientation of the flow towards the south-eastern corner and its acceleration, to reach there the maximum velocity.

The inexistence of recirculation around the obstacle is a consequence of the strong wind forcing and (as it will be seen further down) of the OBC. The strong wind shear creates a free surface depression behind the obstacle, which together with the free surface distribution created by the OBC generates an inshore water flow downstream of the obstacle. This flow eliminates the recirculation downstream of the obstacle. Further down it will be shown that using a radiative OBC a recirculation is generated by the model. A detailed view of the flow field around the obstacle's northwest corner is presented in Figure 6. The figure shows a stagnation zone off the obstacle, but no clear recirculation. Again the explanation seems to be the high wind shear drag.

In Figure 7, time series of free surface elevation at stations P1, P2, P3, and P4 are shown. All stations present some high frequency variability (noise) which is associated to the interaction between the initial conditions and the imposed boundary conditions which reflect initial perturbations. After the third day of simulation these oscillations have been dissipated and a clear longitudinal free surface elevation can be seen in the figure.

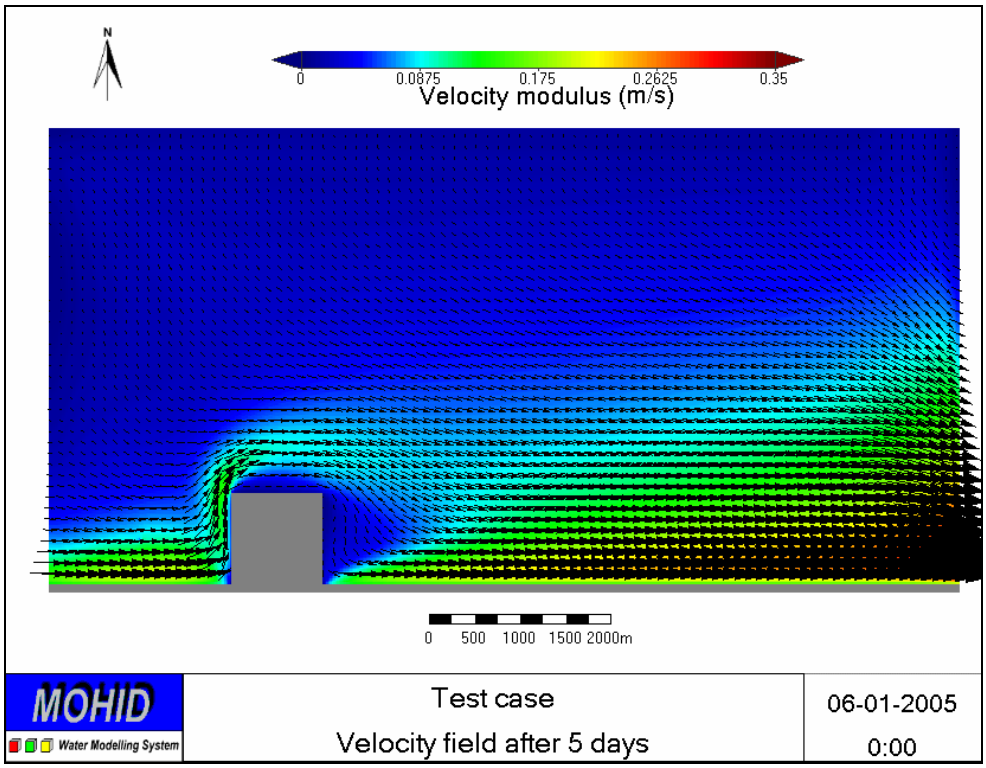

Figure 4 – Test-case - Velocity field after 5 days of simulation (velocity arrows plotted every 6 grid cells)

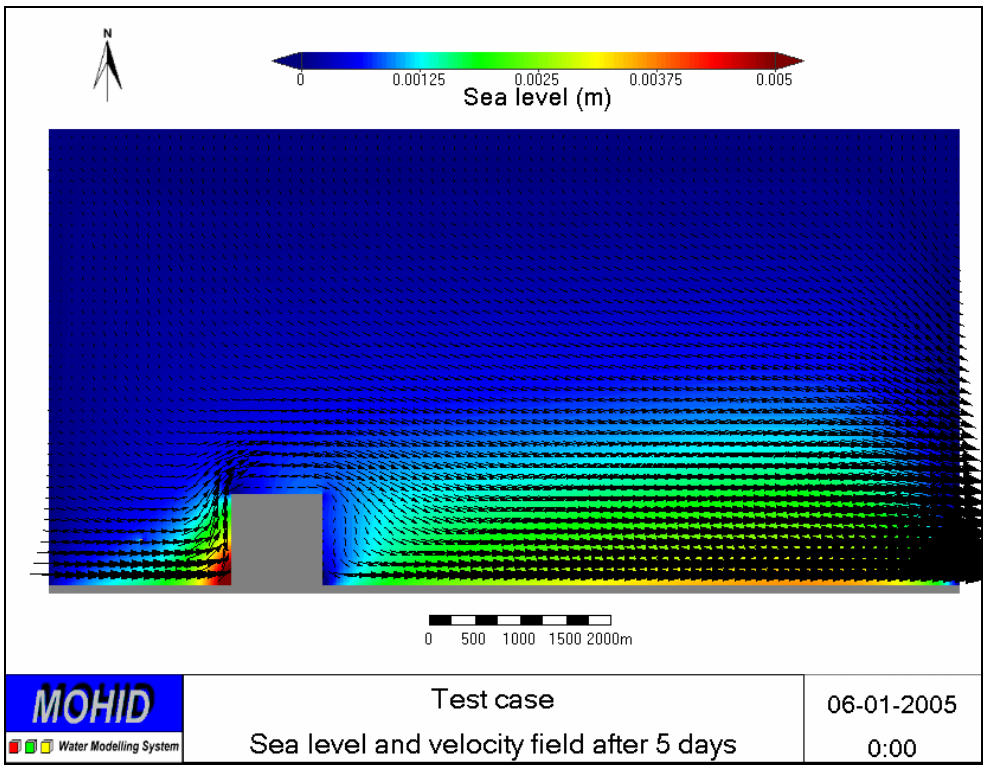

Figure 5 – Test-case – Free surface elevation and velocity field after 5 days of simulation (velocity arrows plotted every 6 grid cells)

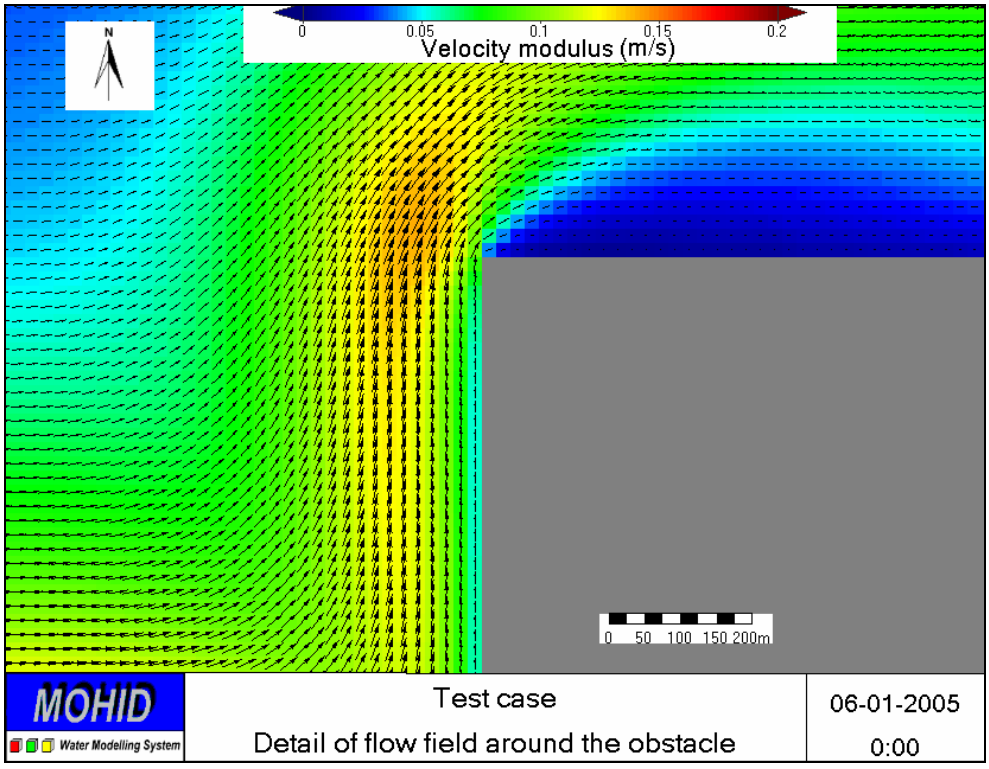

Figure 6 – Detail of flow field around the obstacle after 5 days of simulation

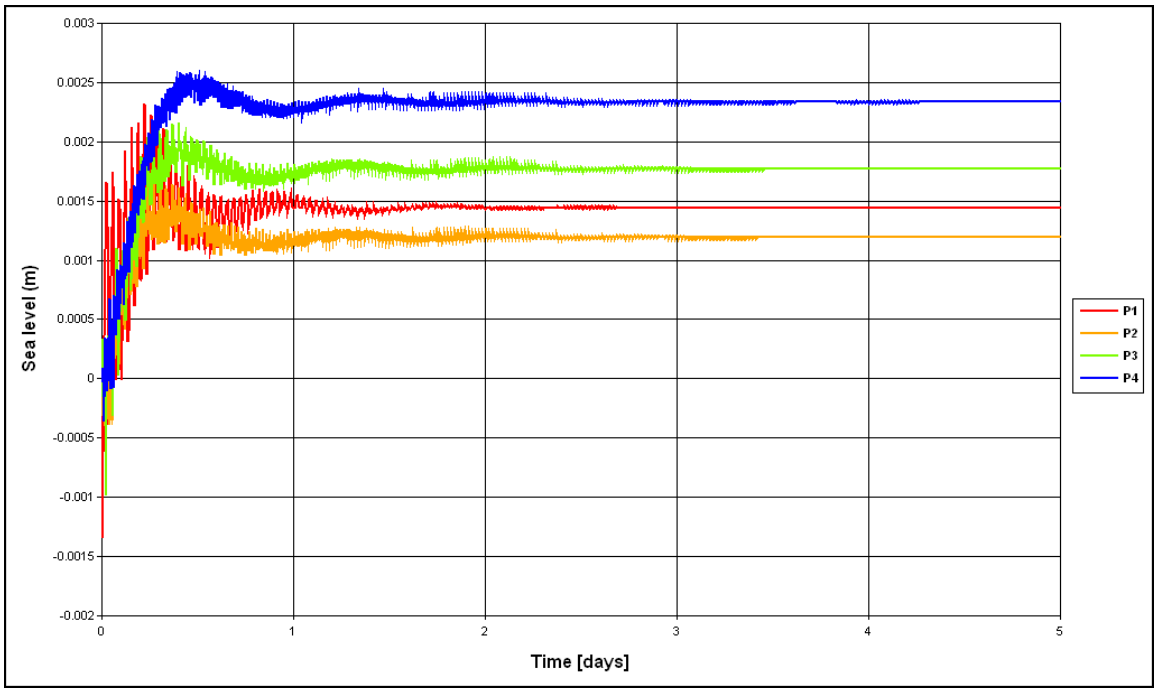

Figure 7 - Evolution sea level in the selected locations

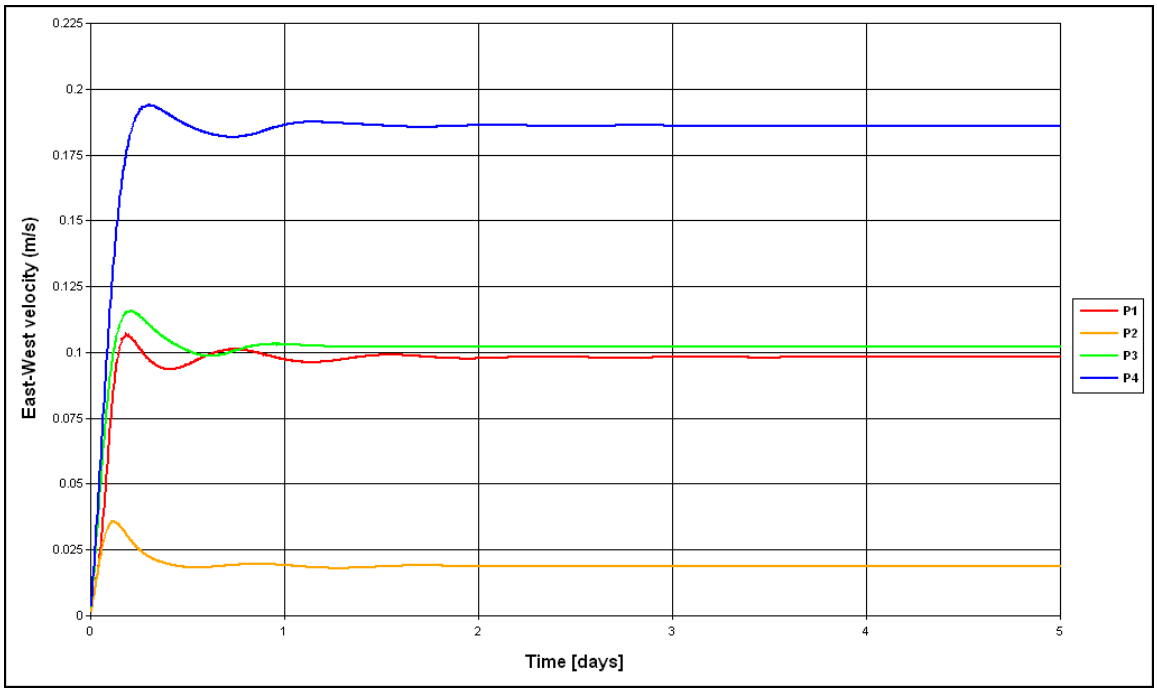

Figure 8 - Evolution East-West velocities in the monitoring stations

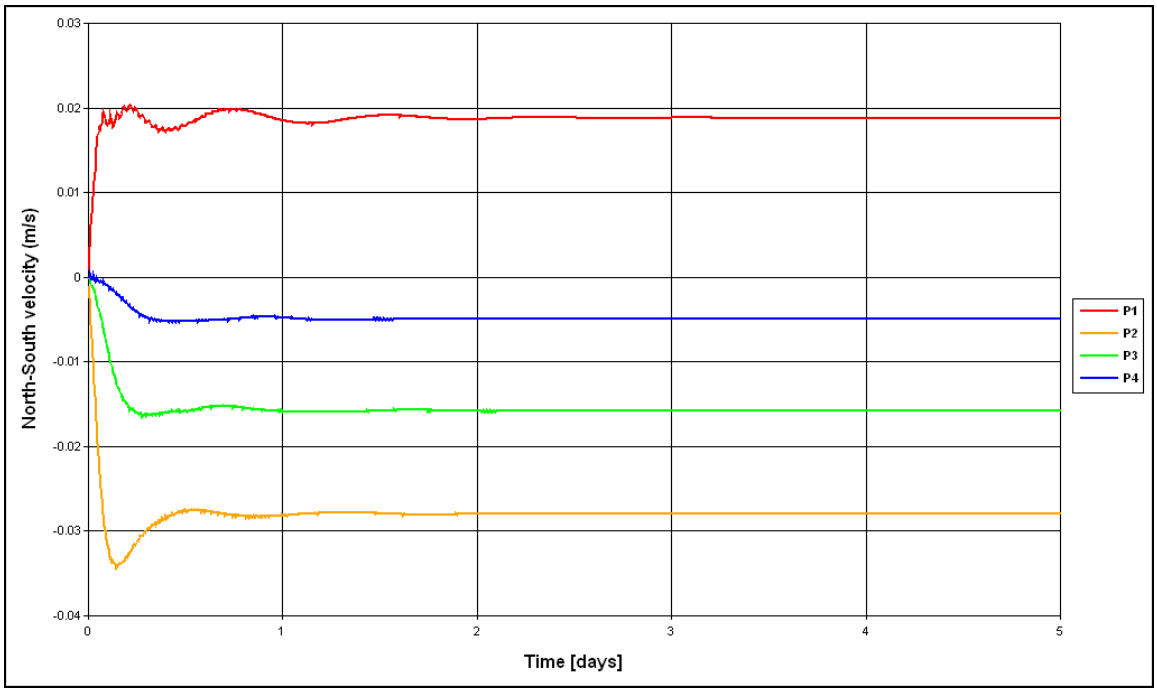

Figure 9 - Evolution of South-North velocities in the monitoring stations

Figure 8 and Figure 9 present respectively the evolutions of westward and northward velocity components in the stations P1, P2, P3 and P4. Again, a stabilization period is shown, although the high frequency waves are less clear, as expected.

Figure 10 presents the contaminant concentration evolution in the monitoring stations. The concentration in the domain stabilizes after the second day, being the values in downstream points very low (around 10 mg/l), when compared with the concentration

at the discharge (10^6 mg/l). The residence time of the plume between the discharge and the eastward point is around 6 hours, which is in the same order of magnitude of the contaminant decay time, T_{90} (5 hours). By the time the contaminant reaches P4, its concentration has been reduced in five orders of magnitude, which, if concentration decay was only dependent on T_{90}, it would take 5 times longer. Thus, dilution is clearly the main process responsible for concentration decay. Figure 11 presents a spatial distribution of the contaminant concentration, after 5 days of simulation. The small length of the plume is clear.

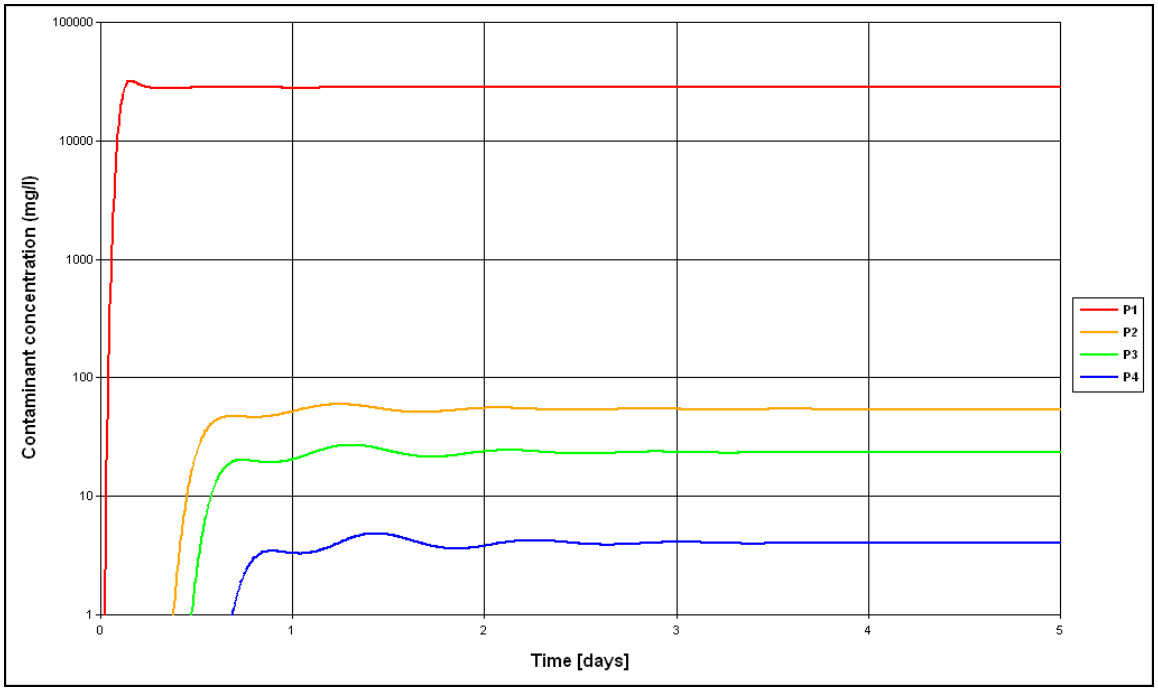

Figure 10 - Evolution of contaminant concentrations in the selected locations

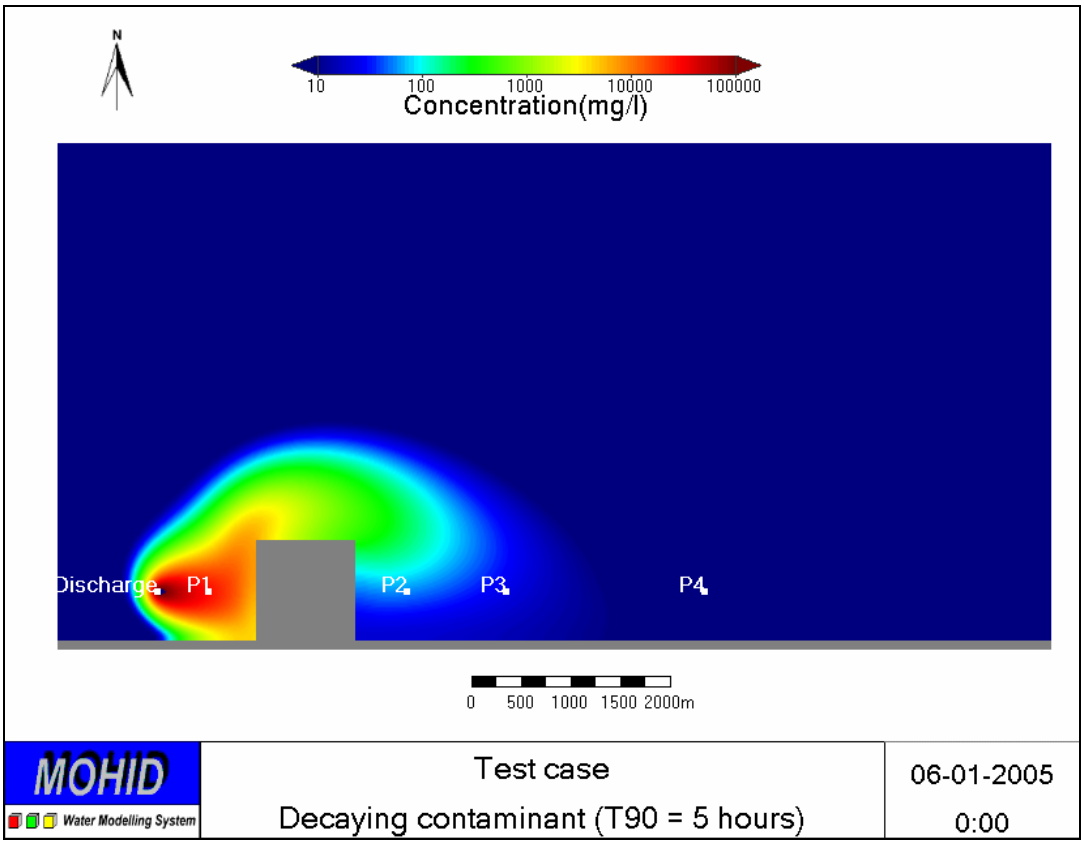

Figure 11 – Contaminant concentration field after 5 days of simulation.

4.1.2 About the Runs

The simulation was done in a PC running on Microsoft Windows XP Professional, equipped with a 3.4 Ghz Intel Pentium IV Processor and required 100MB RAM. The run took around 9 hours of CPU time. The model was compiled with Intel FORTRAN Compiler 9.0. The time required for implementing the test case and preparing the figures was about 2 days*person.

5. Alternative Hydrodynamic Model Setup

In chapter 3 were presented results obtained using the boundary conditions suggested in the questionnaire and it was shown that OBC used for hydrodynamic simulations are determinant for the solution obtained. In order to test the sensitivity of the solution to the boundary conditions and to the number of dimensions of the model, two extra simulations were done. In one, all the options were maintained, except the hydrodynamic boundary conditions, where a cyclic boundary condition was used. In the other simulation this boundary condition was used with a three dimensional discretization.

5.1 Cyclic Open-Boundary Condition

The test-case simulated with imposed sea level and velocity at the open boundary represents a problem where local wind is the exclusive responsible for the flow. Inside the domain the flow adapts to the topography (slope and promontory) and to the OBC imposed.

Another schematic situation would be the case of an infinite rectilinear coast with a uniform slope where a uniform wind generates a flow parallel to the coast and where a topographic accident generates a local perturbation. This case was simulated benefiting from the great variety of open boundary conditions for flow and water properties available in MOHID: imposed value, null gradient, radiative, cyclic, flow relaxation scheme and hybrid combinations of the previous options.

The sea level imposed OBC admitted for the test case generates an artificial south-eastern flow close to the eastern boundary that by geostrophic balance piles up water near the east boundary. This effect is well illustrated in Chapman (1985) where the author also tests many other OBC for a case similar to this one. An analogous work is done in Palma and Matano (1998) and in Leitão (2003). The latter describes in detail the OBC options adopted in MOHID.

The next paragraph explains how the cyclic OBC associated to a nesting method can avoid the artificial flow close to the eastern boundary, giving a better view of the effect of a topographic feature on a general flow parallel to a rectilinear coast.

5.1.1 Model setup

In the present case, the aim is to simulate the effect of a topographic feature over a flow parallel to a rectilinear coast. For that purpose two boundary conditions were

associated: A cyclic boundary is used to obtain the background flow along the infinite coast (level 1 solution) and a sub-model is nested inside this global solution (level 2 solution) using a radiative boundary condition which allows the radiation of the difference between the actual solution and the background solution at the boundary. For this purpose a “one-way” nesting approach is appropriate. Also, a bottom friction coefficient is computed assuming a logarithmic velocity profile and a rugosity of 2.5 mm).

Figure 12 shows how the two levels are combined. The first level was run with a cyclic boundary condition and a bathymetry similar to the test case (shown on the left) but larger and without the obstacle. This level used a coarser grid: 100 m x 100m. The second level was run with the test case bathymetry and resolution (on the right in the figure) and using the Flather (1976) radiation OBC having level 1 solution as the reference solution. Both levels run simultaneously using a 5 seconds time step (Courant number of 20).

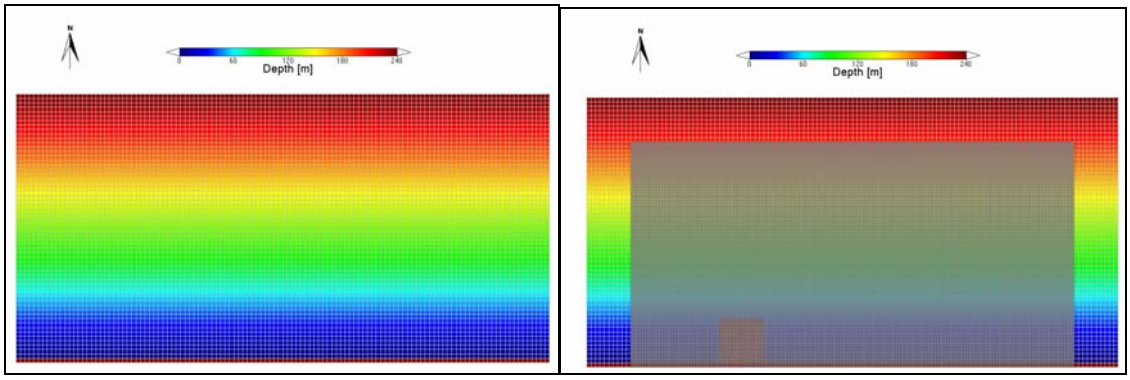

Figure 12 – a) level 1 bathymetry; b) level 1 bathymetry overlapped by level 2 bathymetry.

5.1.2 Results

Figure 13 displays level 1 velocity field overlapped by the level 2 field, showing that there is no discontinuity between both solutions. Comparison between this figure and Figure 5 shows that the artificial free surface gradient close to the eastern boundary has been eliminated and that velocity increased in deeper areas. Free surface level distribution around the obstacle has similar patterns.

Higher velocities in the deeper areas are a consequence of the infinite length of the domain and of the lower relative rugosity. As a consequence of the higher intensity of the flow, the obstruction of the coastal promontory is higher and generates higher accelerations. That is shown in Figure 14. The figure show vectors only for small velocities around the obstacle (smaller than 10 cm/s). The figure puts into evidence areas of high velocity gradients and the recirculation downstream of the obstacle.

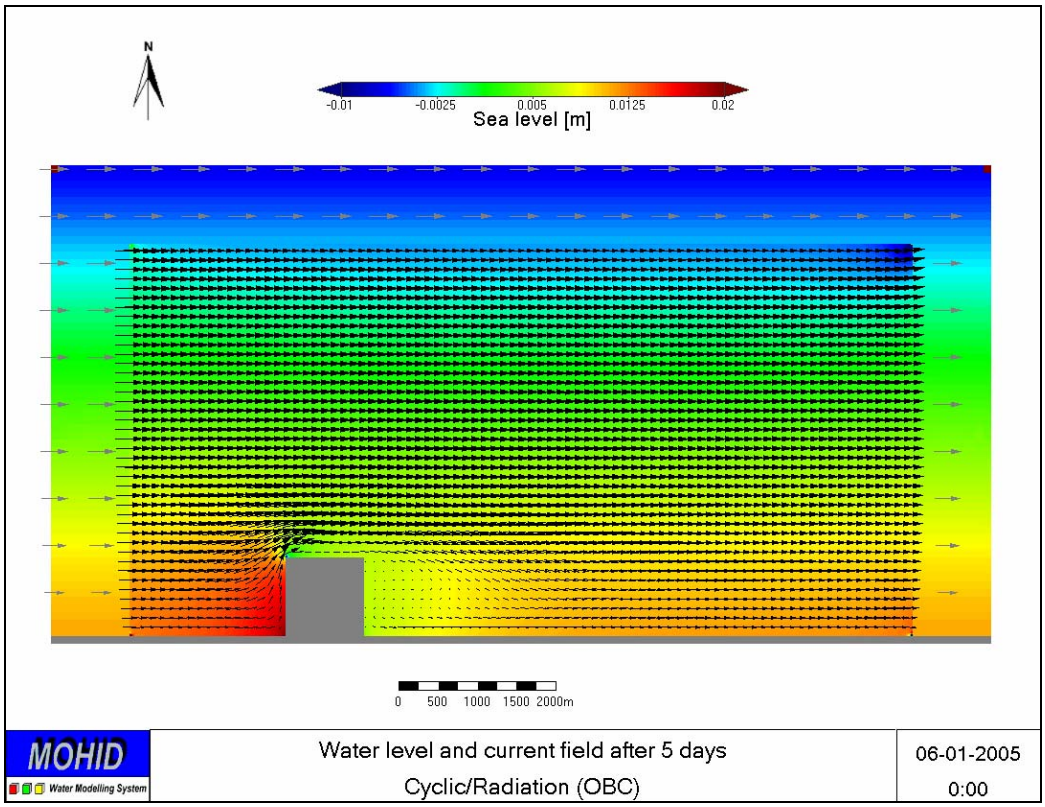

Figure 13 – Velocity field of level 1 overlap by the level 2 solution. Vectors are plotted every 6 cells.

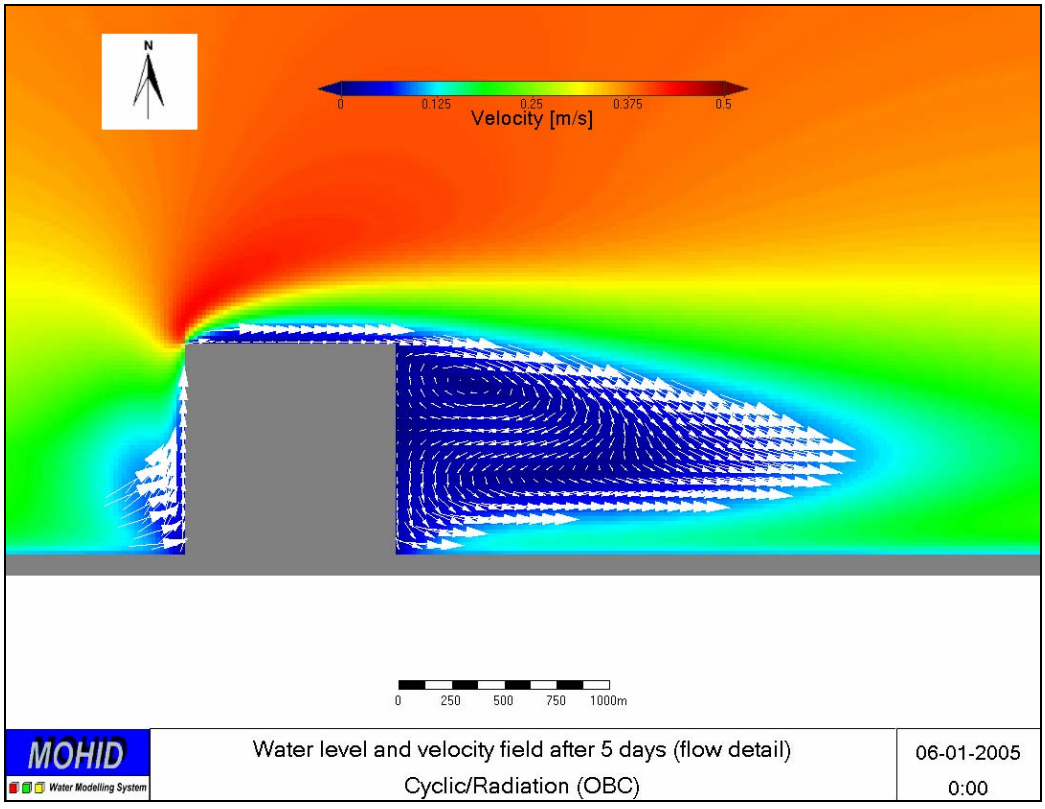

Figure 14 – Detail of the circulation immediately downstream of the obstacle. Vectors are plotted every 3 cells. Vectors are only plotted for intensities lower than 10 cm/s.

As a consequence of the flow pattern, the distribution of the contaminant is much different, with a longer plume and higher concentrations at stations downstream of the obstacle. Dilution is high close to the obstacle due to shear diffusion, but decaying is less effective resulting in higher concentrations downstream. In this case the residence time of the plume is similar to T_{90}.

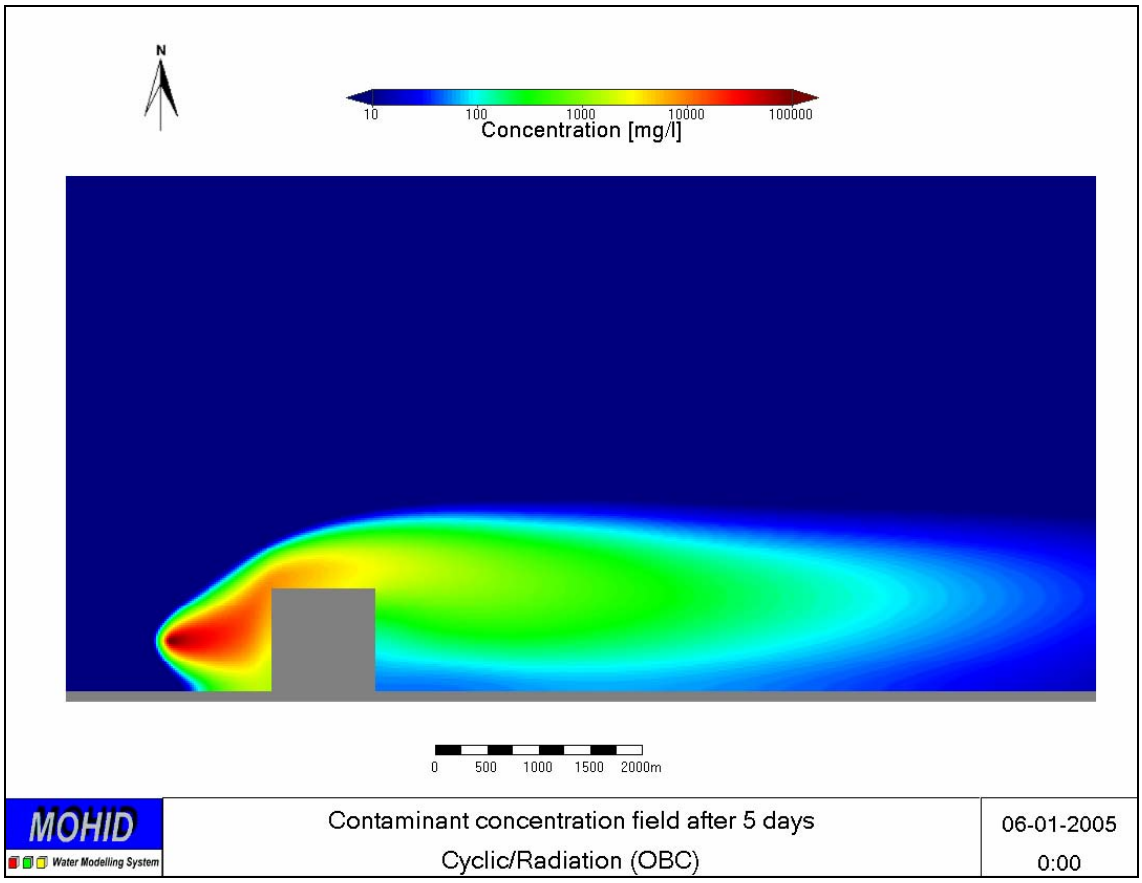

Figure 15 – Contaminant plume with a first order decay (T90 = 5 hours).

5.2 3D Simulations

The discharges in coastal waters associated with Combined Sewer Overflows can generate important 3D hydrodynamic processes that can be enhanced by the surface wind forcing. In this case this is particularly important because a discharge of 50 m^3/s is of the same order of magnitude of many rivers' discharge and only one order of magnitude lower than the average Tagus river discharge. For evaluating the importance of the vertical processes a three dimensional study was carried out. OBC is imposed as in paragraph 5.1.

5.2.1 Model setup

The three dimensional simulations were carried using 10 equally distributed sigma layers and a spatial step of 100 m. Discharge and receiving water salinities were assumed to be 0 and 39 psu respectively. Vertical turbulence diffusivity was computed using the GOTM k-ε model[1], using the parameterization proposed by Canuto et al. (2001).

5.2.2 Results

Results are presented for hydrodynamics and for transport. In case of transport simulations done using eulerian and lagrangian approaches were compared.

5.2.2.1 Hydrodynamics

Figure 16 and Figure 17 show the surface and bottom velocity fields respectively, after a 5 days simulation. The comparison of the figures shows a clear vertical velocity gradient, with velocities that can reach 60 cm/s on the plume. This effect shows that the stratification due to the fresh water input inhibits vertical diffusion, increasing the vertical gradient.

Another interesting feature can be observed near the discharge, in a localized area, where there is a convergence of the bottom water to the jet and its divergence at the surface and the fact that recirculation is not visible at the surface and stagnant area increased close to the bottom. Salinity distributions at the surface and close to the bottom are shown in Figure 18 and in Figure 19. The results show that the salinity

[1] MOHID is coupled to the General Ocean Turbulence Model (GOTM) which includes several standard turbulence models (Burchard and Bolding, 2001).

plume does not reach the bottom, except in the closer corner, upstream of the obstacle where the vertical flow pattern is more complex.

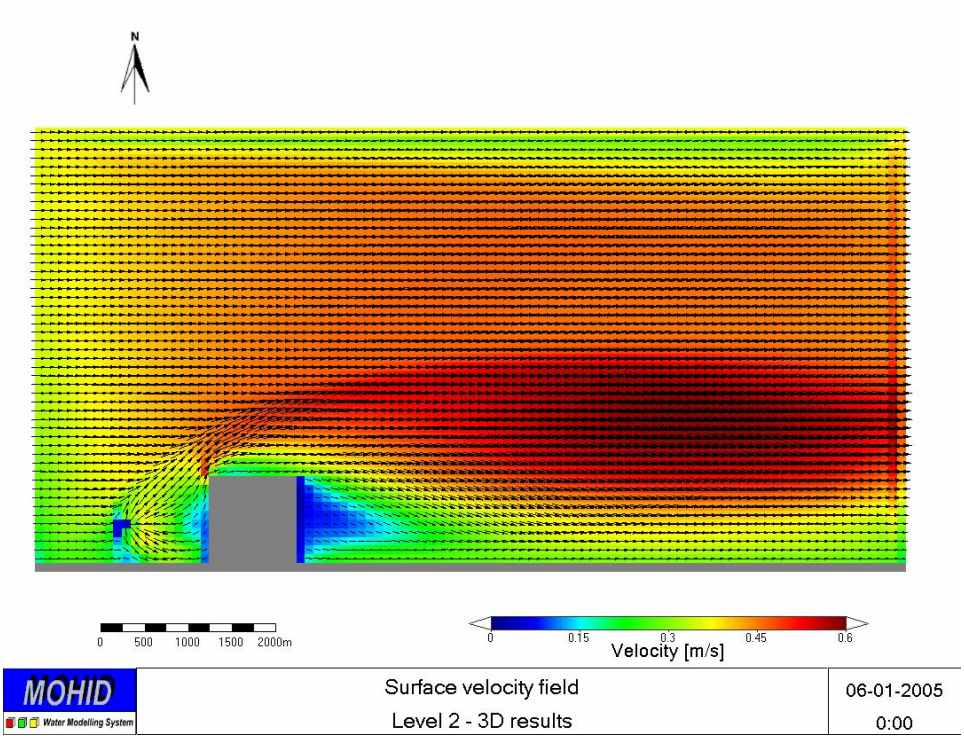

Figure 16 – Surface layer velocity field after a 5 days run. Vectors are represented in every cell.

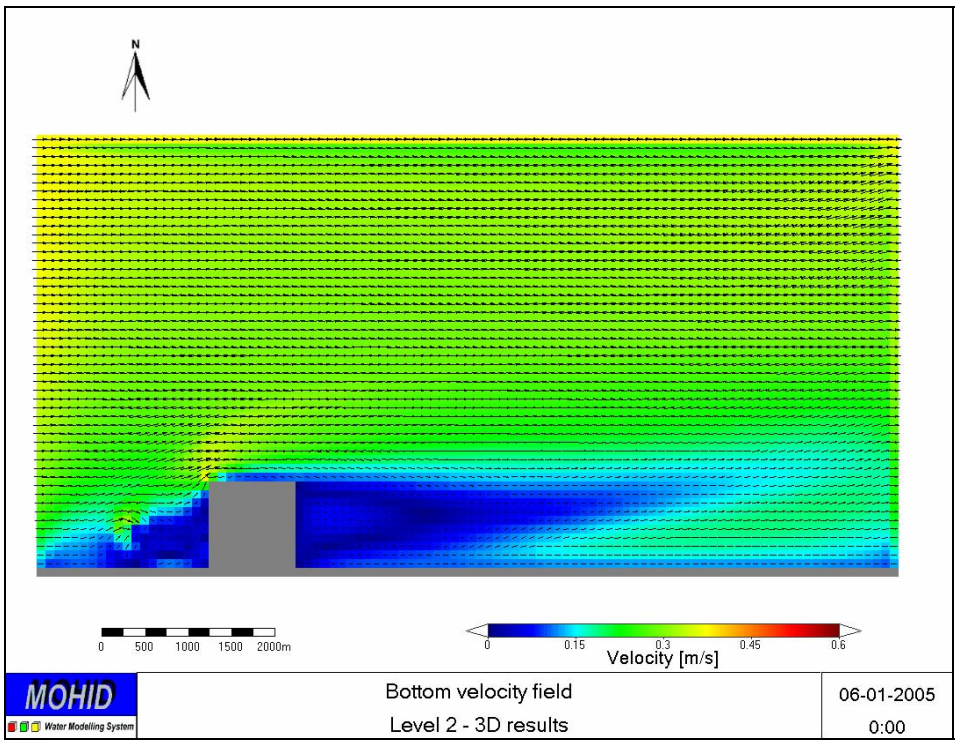

Figure 17 - Bottom layer velocity field after a 5 day run. Vectors are represented in every cell.

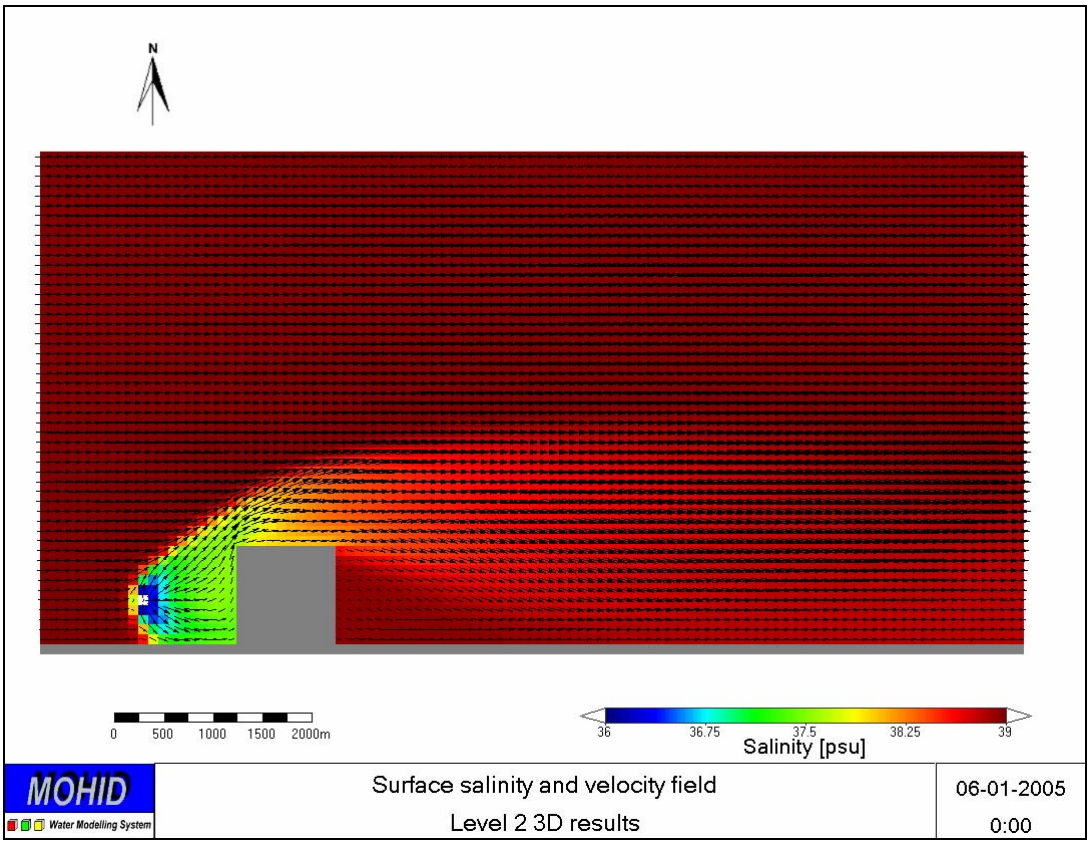

Figure 18 – Surface layer salinity and velocity field for the level 2 domain

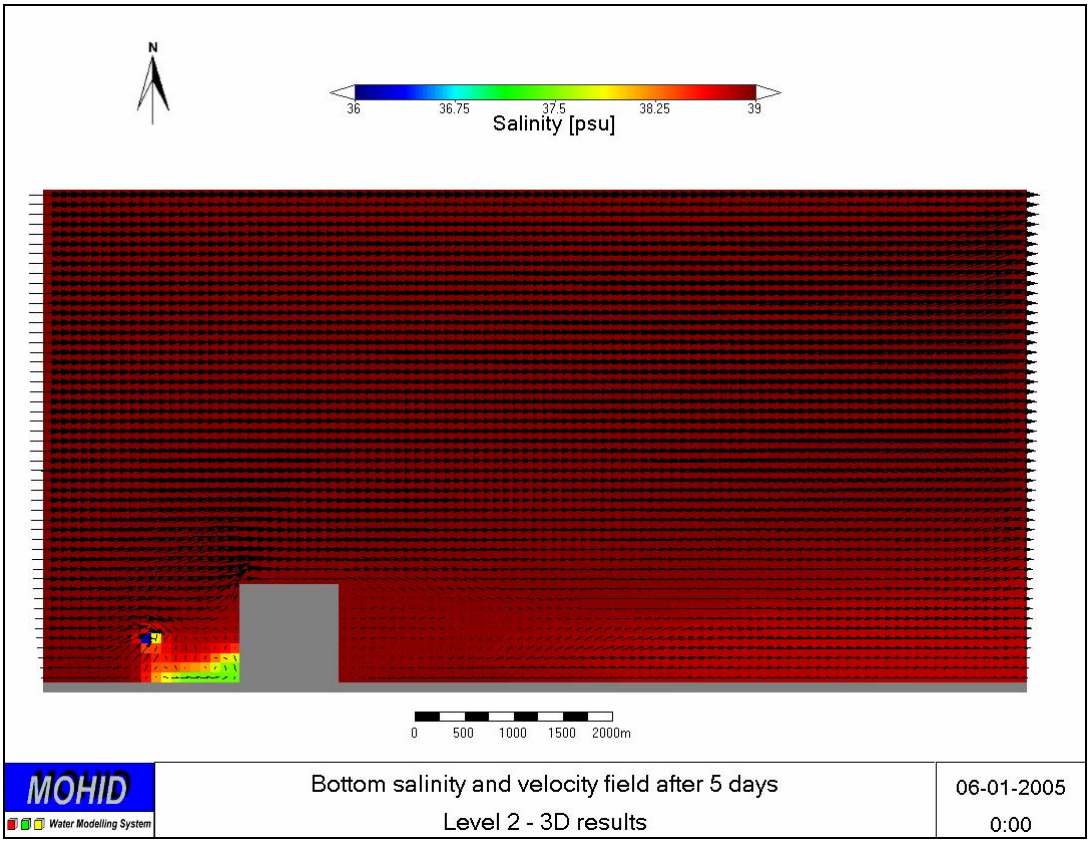

Figure 19 – Bottom layer salinity and velocity field for the level 2 domain.

Figure 20 compares the surface velocity computed by the 3D model (black vectors) with the 2D solution (red vectors) and Figure 21 does a similar comparison for the bottom. The divergent flow at the surface and the convergent flow at the bottom due to the jet buoyancy effect are clear in the 3D simulation. The comparison of the two figures put into evidence (1) the presence of a secondary flow along the upper left corner of the obstacle identifiable by a “off the obstacle” difference between 2D and 3D at the surface and a “in the obstacle” difference at the bottom and (2) the effect of density stratification downstream of the obstacle that clearly increments the surface velocity relatively to the 2D case. The surface velocity increase is due to the fact that stratification blocks the vertical mixing of momentum supplied by the wind stress.

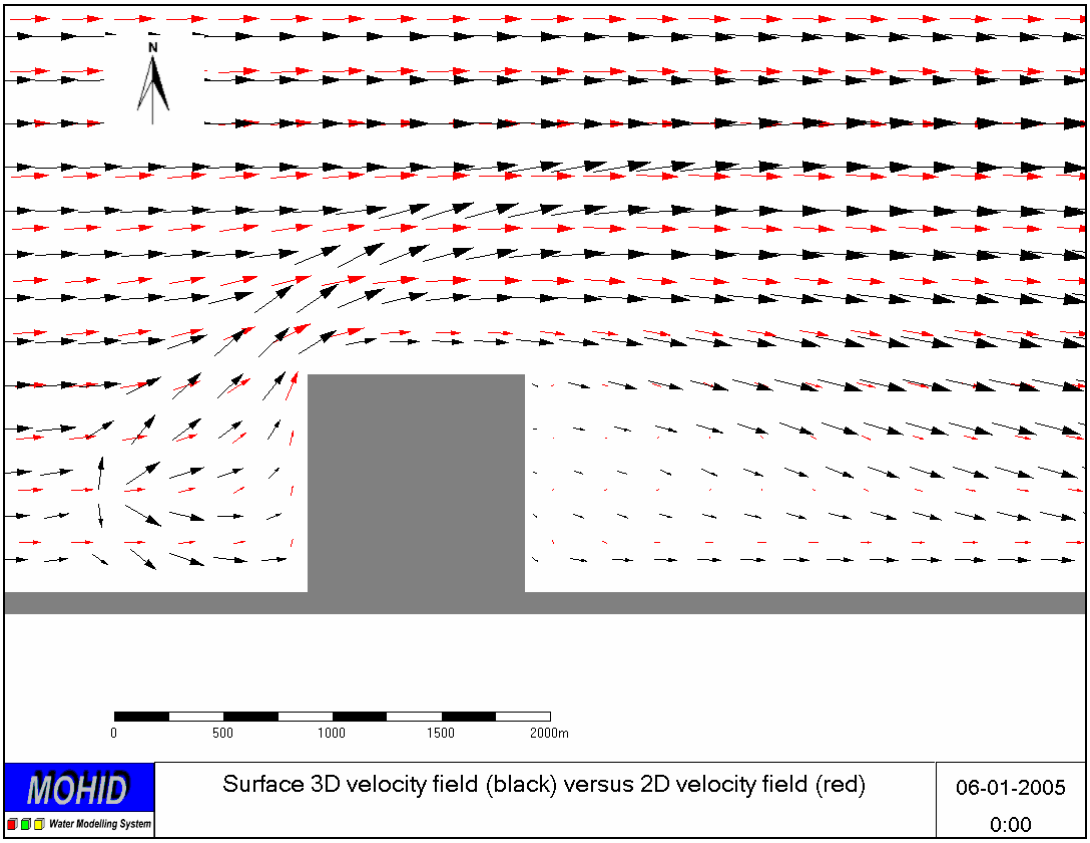

Figure 20 – Surface layer velocity field for the 3D case (vectors in black) overlapped by the 2D case (vectors in red).

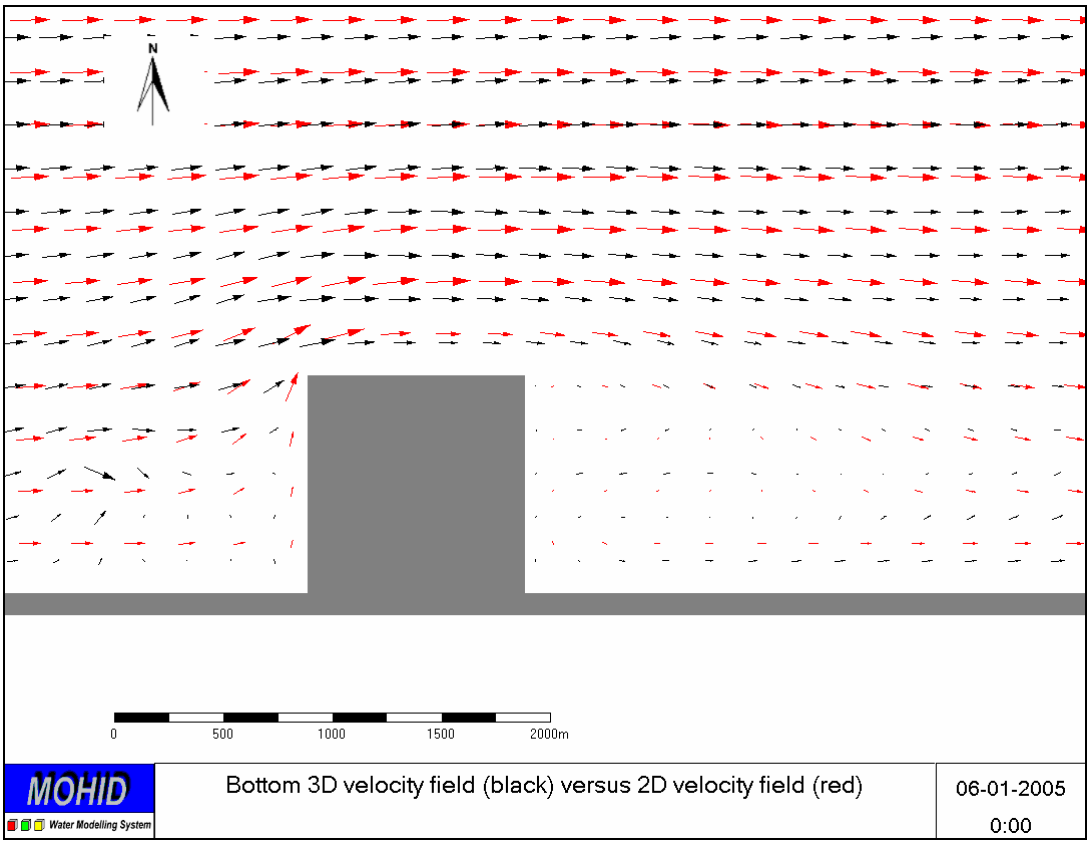

Figure 21 - Bottom layer velocity field for the 3D case (vectors in black) overlapped by the 2D case (vectors in red).

5.2.2.2 Transport Processes

MOHID Water Modelling System has two transport modules used to compute the movement of water masses: one eulerian and another lagrangian. The lagrangian module can be used for computing concentrations in situations with very high gradients and where numerical diffusion of eulerian methods can compromise the results. Results using both approaches are presented below.

Results are shown from Figure 22 to Figure 25. Globally the results obtained by the two simulations are similar, showing that in this case the grid is fine enough for performing accurate eulerian simulations. At the surface, Figure 22 and Figure 23 the results are very close, the eulerian's solution being smoother, as expected. Close to the bottom (Figure 24 and Figure 25) the differences are more evident although they remain small, because concentrations are small.

In this case the lagrangian simulation has no benefits because the plume occupies about ½ of the domain. The lagrangian simulation becomes more interesting when the plume is much smaller than the domain. In this application the number of tracers (~90.000 in stationary conditions) was chosen to be in the order of magnitude of the

number of eulerian model cells (50.000). If the plume was 1/20 of the model surface (a common situation in real cases) lagrangian results would be better than eulerian results. An added value of the Lagrangian simulations is the capacity of tracking the water that passed in a point. This is particularly interesting when there are several sources of a contaminant whose fate has to be tracked. Another added value is the capacity of tracking the water that passed by a point. Figure 26 shows the location of the tracers that were emitted by the discharge.

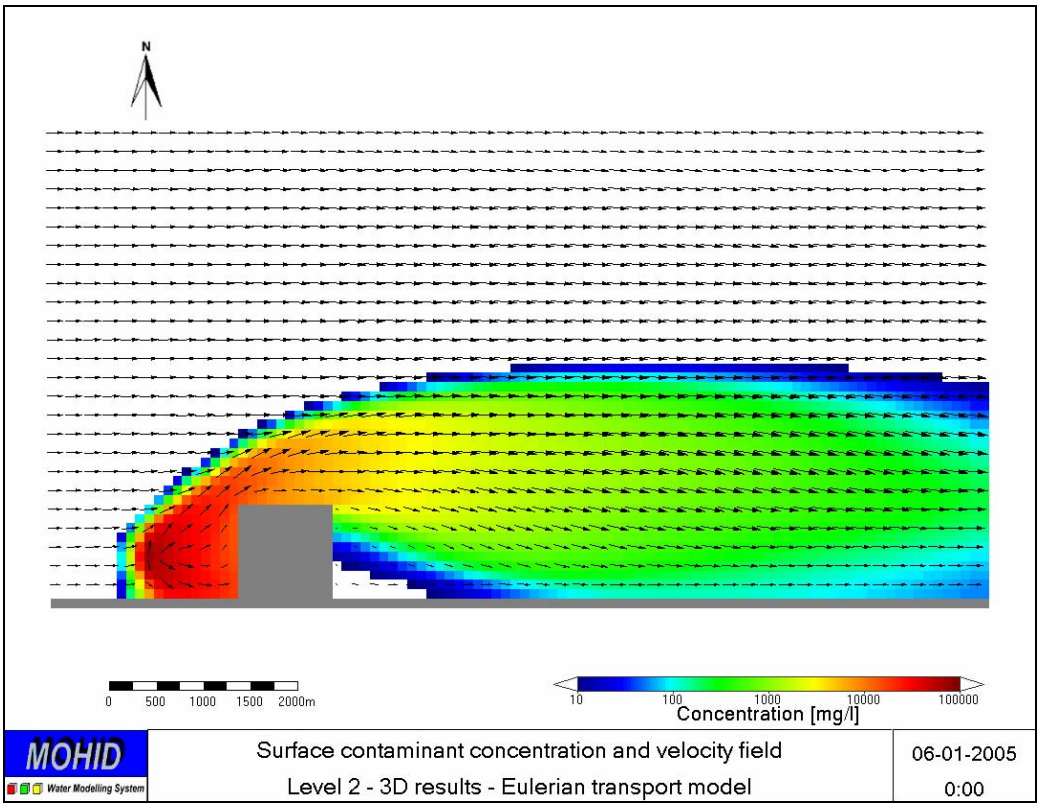

Figure 22 – Surface layer contaminant concentration (eulerian results) and velocity field.

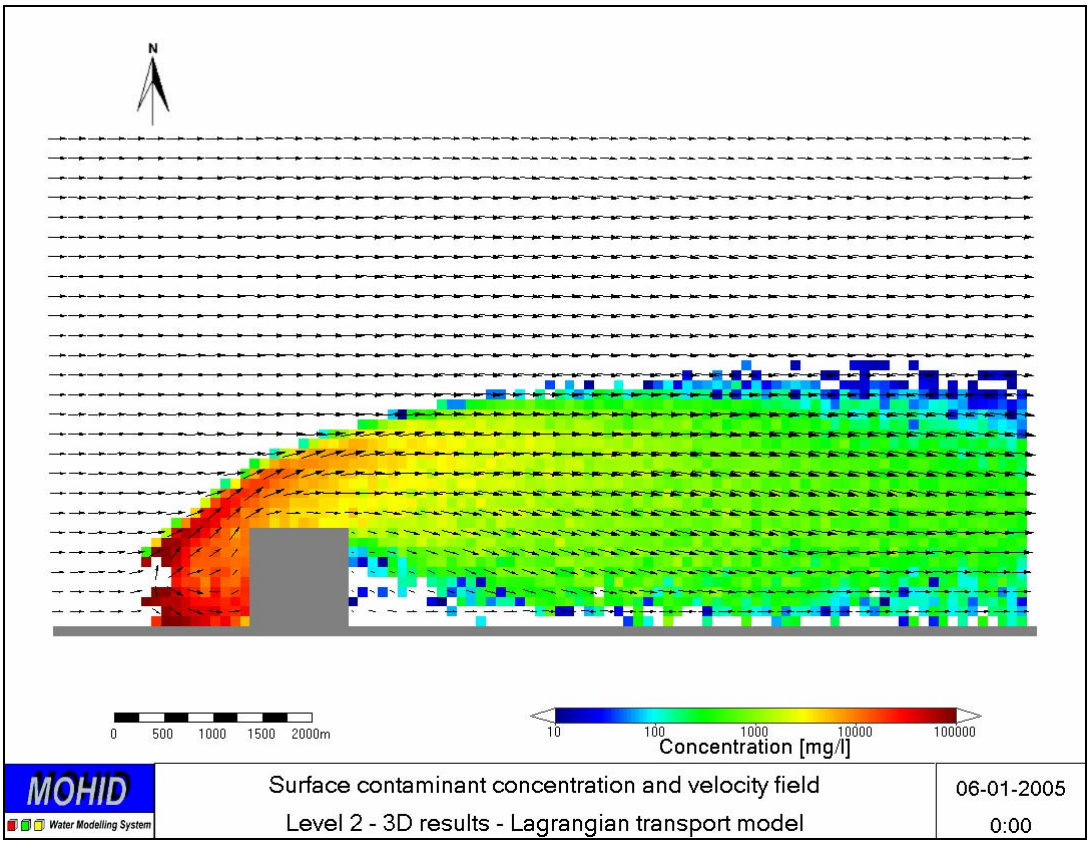

Figure 23 – Surface layer contaminant concentration (lagrangian results) and velocity field.

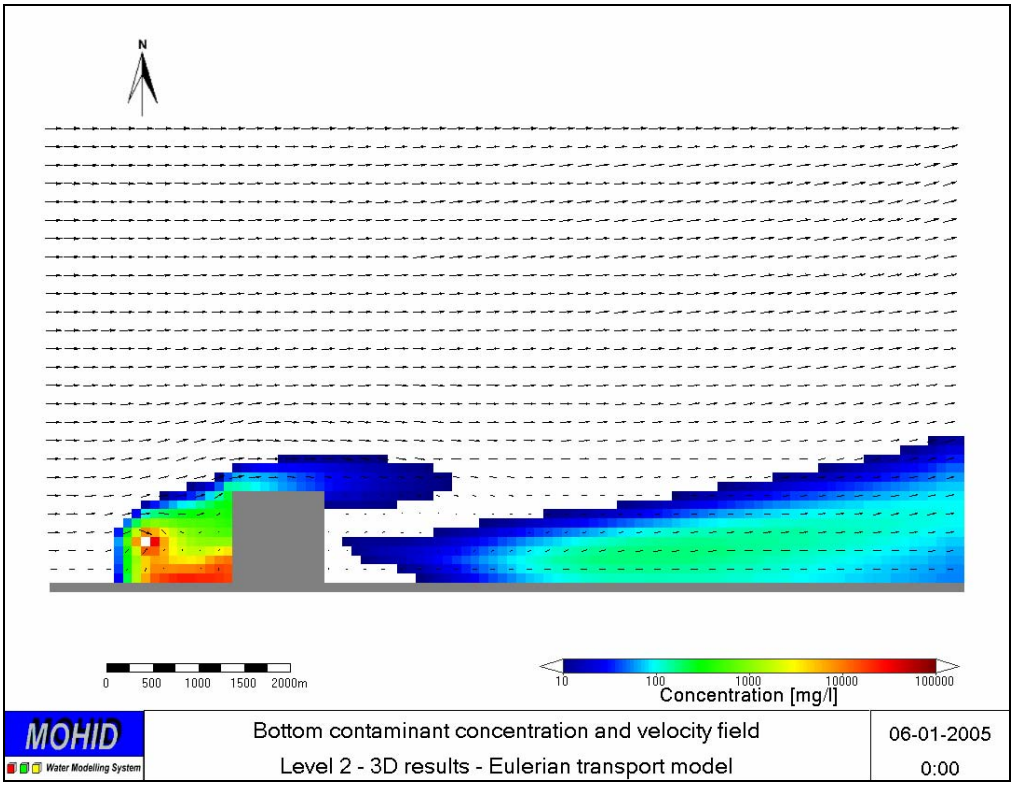

Figure 24 – Bottom layer contaminant concentration (eulerian results) and velocity field.

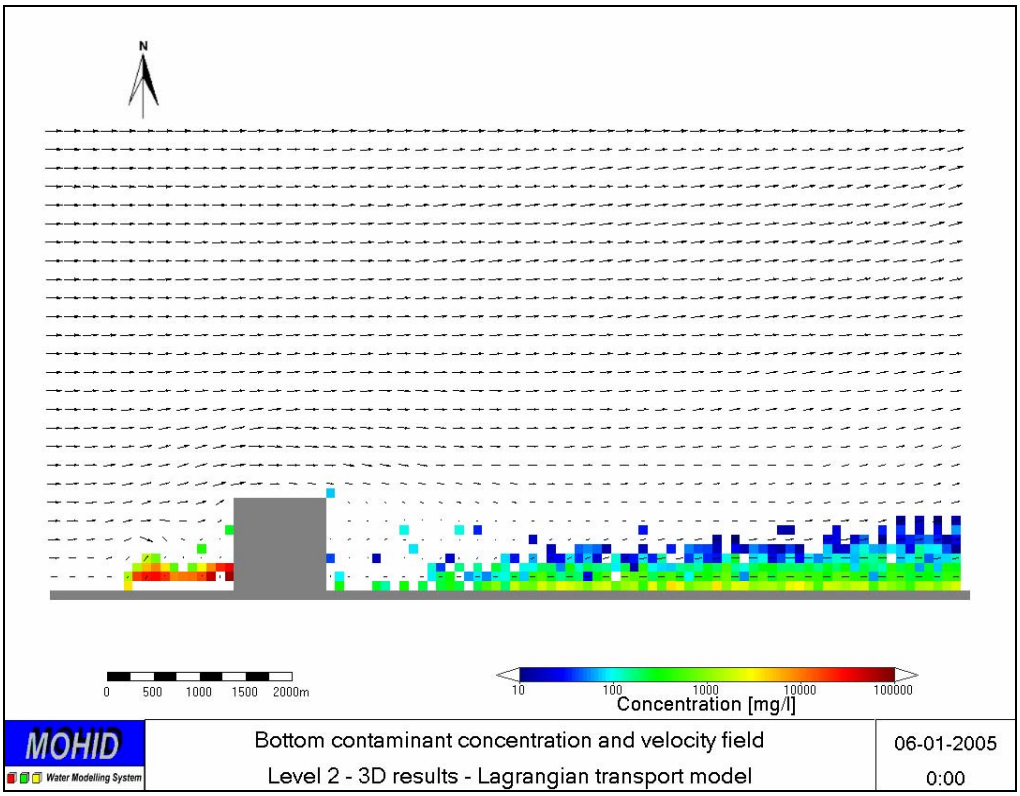

Figure 25 – Bottom layer contaminant concentration (lagrangian results) and velocity field.

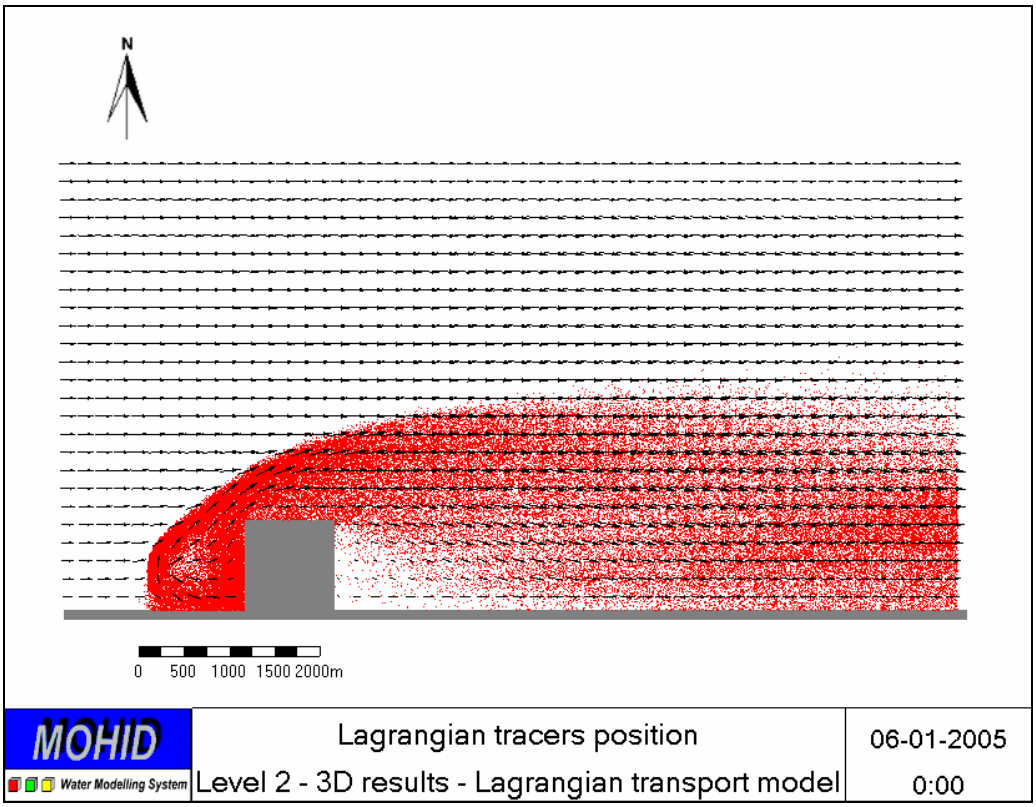

Figure 26 – Velocity field and in red are presented all the tracers position (their number is of the order of 90.000).

6. Biogeochemical Simulations

Biogeochemical modelling of the fate of material discharged in point sources is usually a small overhead in terms of CPU time. In fact, the most time consuming activity is the simulation of hydrodynamics and transport processes, which require most geographical data processing and the main definition of modelling scenarios (including boundary conditions selection). For those reasons it was decided to complement the hydrodynamic and transport simulations with some biogeochemical simulations.

Simulations have been done for the 3D scenario. The impact of an urban waste water discharge through a submarine outfall on primary production and related biogeochemical processes was simulated to complement the decaying constituent scenario. This was accomplished by activating MOHID Water Quality Module, which is prepared to simulate nitrogen, phosphorus and silica cycles on top of temperature, salinity and cohesive sediments. In this case only the nitrogen cycle was simulated and results are presented for phytoplankton, ammonia and nitrate. Figure 27 shows the main processes involving phytoplankton and the state variables. In this case silica is not a limiting nutrient.

Water quality simulations are easy to carry on in MOHID because the ecological processes - sink and source terms of the transport module – have been implemented in a “zero dimensional” formulation and does not have to know anything about the geometry of the problem. This makes it also possible to use the same formulation both in Eulerian and Lagrangian formulations (Pina, 2001).

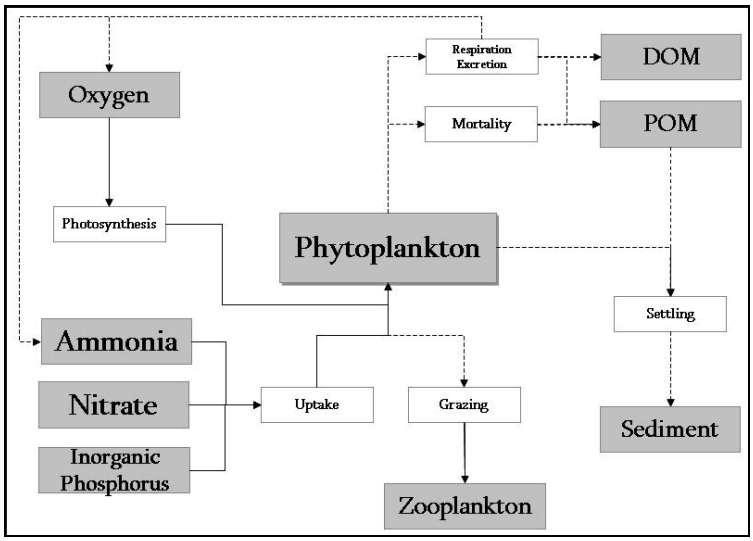

Figure 27 – MOHID Water Quality Module: Main processes involving phytoplankton.

6.1 Model setup

In order to illustrate the impact of the plume, very small concentrations were considered in the receiving waters, while the water discharged was assumed to be a typical domestic effluent (this is not a realistic situations having in mind the fact that 50 m^3/s are being discharged). In this schematic case only the nitrogen cycle was simulated and consequently constant C:N:P[2] ratios are assumed.

Both level 1 and level 2 models (father and son) time step was set to 15 seconds. The model was run for 5 days in 3D mode (100x100m grid), using the cyclic boundary condition approach, for hydrodynamics and an imposed value for water properties.

The model was parameterized using the default options, which can be found in the model's technical manual (http://www.mohid.com). The model was setup to simulate one phytoplankton species, one zooplankton species, the nitrogen cycle and oxygen.

The concentrations in the effluent – see Table 2 - were assumed to be the typical concentrations discharged by the Guia submarine outfall in Estoril, near Lisbon, Portugal, which serves around 700.000 inhabitants (2 to 5 m^3/s)[3].

In order to maximize the ecological processes, namely primary production, the simulation period was defined from June, 1st to June, 6th, so that favourable light conditions are present. Thus, in terms of meteorological forcing, the model used the conditions present in Table 3.

The depth to which light will penetrate in water, and hence the depth at which primary production can occur, is dependent on a number of factors; including absorption of light by water, the wavelength of light, transparency of water, reflection from the surface of the water, reflection from suspended particles, latitude, and season of the year. In this test case, a combined method (Pina, 2001) to compute light extinction in the water column was used, where phytoplankton (chlorophyll-a) and cohesive sediments contribute to light extinction.

As the discharge is assumed to have relatively high fine sediment concentrations (200 mg/l), and particulate matter concentration influences light availability, the particle

[2] C – Carbon; N – Nitrogen, P - Phosphorous

[3] MOHID has been used for several years to study the outfall plume dispersion and its impact on water quality on the shores along Costa do Estoril which have intense recreational use.

dynamics was simulated, assuming particulate properties, cohesive sediments and particulate organic nitrogen using the parameters indicated in Table 4.

Table 2 – Discharge and ambient parameters concentrations

Parameter	Discharge concentration	Ambient concentration	Units
Phytoplankton	0.0001	0.001	mg C/l
Zooplankton	0.0001	0.001	mg C/l
Nitrate	14	0.001	mg N/l
Nitrite	0.5	0.001	mg N/l
Ammonia	45	0.001	mg N/l
Particulate organic nitrogen	2.5	0.001	mg N/l
Dissolved refractory nitrogen	0.8	0.001	mg N/l
Dissolved labile nitrogen	1.8	0.001	mg N/l
Oxygen	0.1	8	mg O_2/l
Cohesive sediment	200	1	mg/l

Table 3 – Meteorological conditions used in the biogeochemical simulations

Parameter	Description	Units
Solar radiation	Computed based on climatological formulations	W/m^2
Albedo	0.05	-
Relative humidity	80	%
Air temperature	18	ºC
Cloud cover	50	%

Table 4 – Fine sediment transport parameters

Parameter	Value	Units
Constant settling velocity	0.01	mm/s
Critical shear stress for erosion	0.2	Pa
Critical shear stress for deposition	0.1	Pa
Reference erosion rate	0.00005	Kg_{sed}/m^2s
Initial deposited mass distribution	0	Kg_{sed}/m^2

6.1.1 Results

Results are shown in Figure 28 to Figure 34. Figure 28 show time series of phytoplankton in the monitoring stations. The figure shows a rapid growth between P1 and P2 and periodic solution after day 1, with a clear daily cycle. Growth occurs during the day, when there's light available and, during the night, phytoplankton concentration decreases due to, respiration, excretions, natural mortality and grazing. During the night the concentration at P1 decreases below the initial value, which is also evolving due to the same processes.

The daily cycle is explained by the residence time. In this simulation the typical velocity (after the flow field stabilization) is 40cm/s and consequently the residence time of the plume inside the simulation domain is about 6 hours. This means that all the production of one light cycle is exported during the night. Another consequence of the small residence time is that phytoplankton has no time to consume the nutrients available (see Figure 34).

Figure 29 displays the phytoplankton distribution after 6 hours of simulation. Near the discharge a small diminishing of the concentration is observed due to mixing between the effluent and the receiving waters. Further down an increase of about 20% can be seen after 6 hours of simulation (18h00 day time). Figure 30 shows the results the day after, at 12h00, Figure 31shows the concentration at 18h00 and Figure 32 at 6h00 in the day after. All together these figures put into evidence the transport and production processes that are responsible for the time series shown in Figure 28. Figure 30 and Figure 31 shows the maximum concentration at the eastern boundary putting into evidence the limiting factor by residence time (the concentration increases while the water is inside the domain). Figure 32 shows the effect of the stagnation zone behind

the obstacle, which limits retains the water inside the domain. This extends to the whole shallow area where velocities are weaker.

There is a concentration gradient from deep to shallow areas. That is a consequence of the higher light availability per unit of volume of water and also because in the morning in this area concentration is higher because of the enhanced residence time.

Figure 33 and Figure 34 present, respectively, ammonia and nitrate concentrations at 18h00 when phytoplankton concentrations reached the daily maximum values (and consumption has reached the maximum). The figures show a strong decay in the vicinity of the diffuser and that the plume extends until the eastern boundary. The decaying of ammonia seems to be faster than the decay of nitrate. This is a consequence of the preference of phytoplankton for ammonia and of nitrification. The extension of the plume is a consequence of the short residence time.

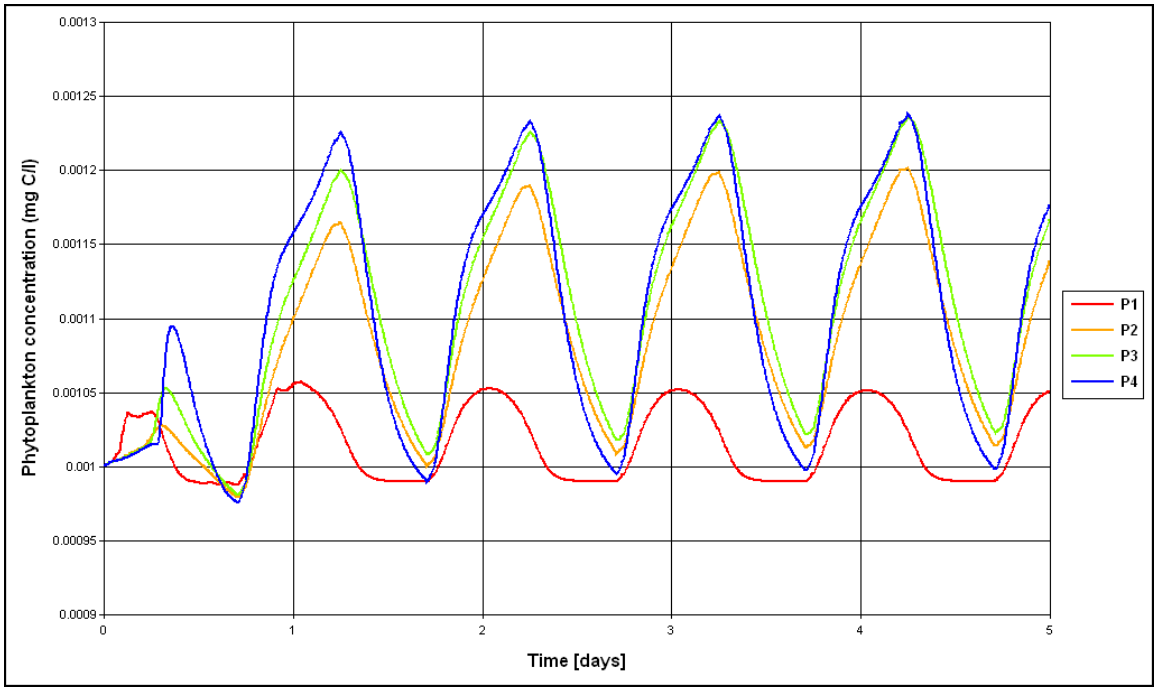

Figure 28 – Phytoplankton concentration evolution in the defined stations. Simulations started at 12h00 and consequently "1 day" simulation is also at noon. Having this in mind it is clear that maximum concentration is reached by the end of the day light.

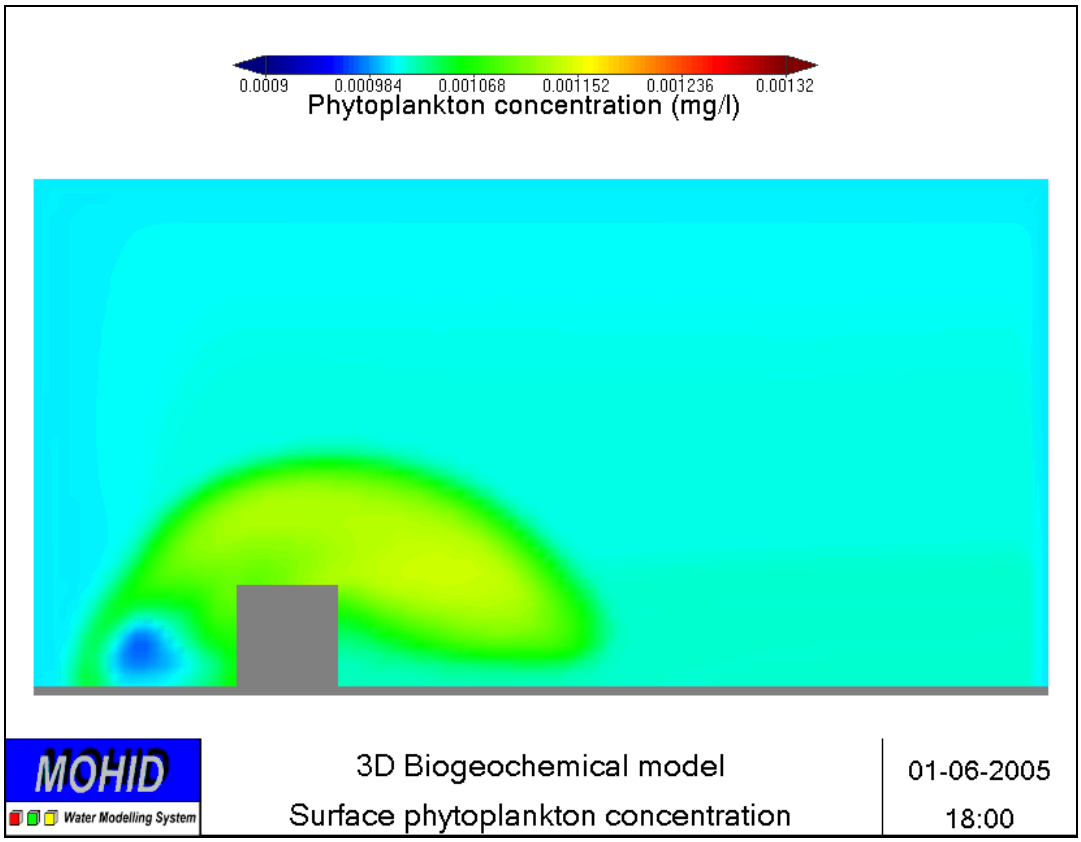

Figure 29 – Surface phytoplankton concentration after 6 hours of simulation

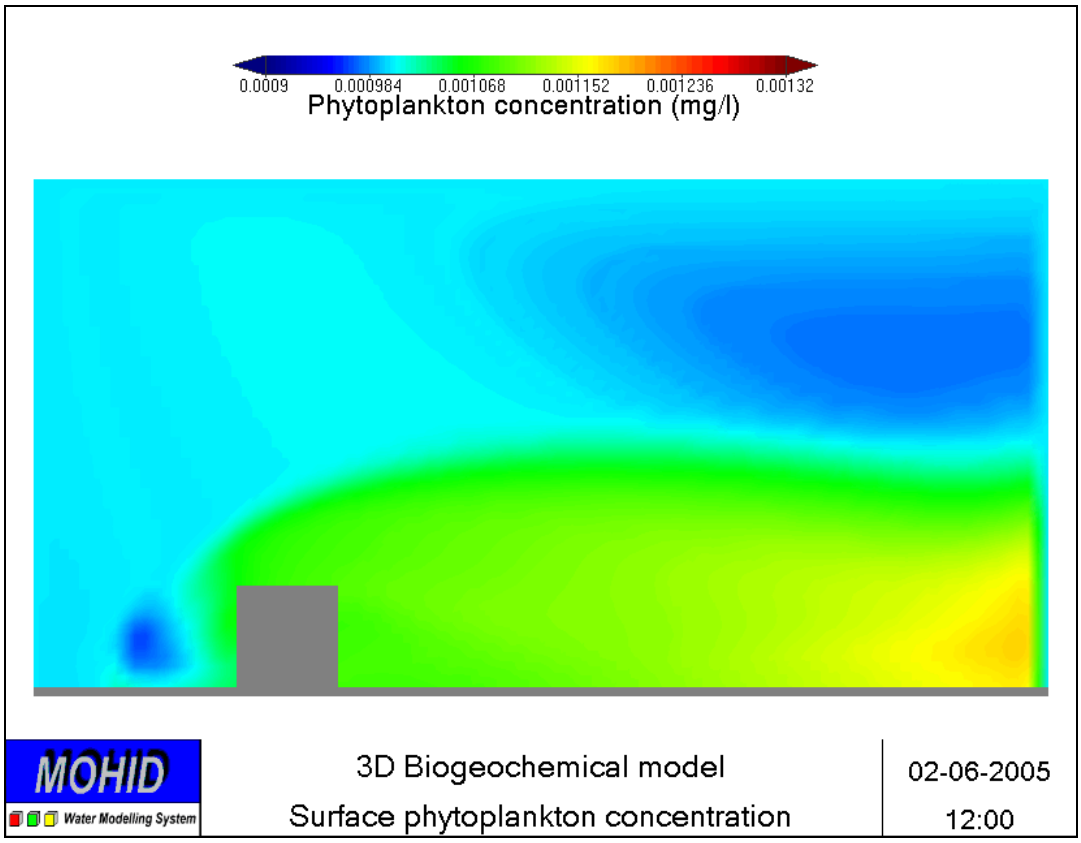

Figure 30 - Surface phytoplankton concentration after 24 hours of simulation

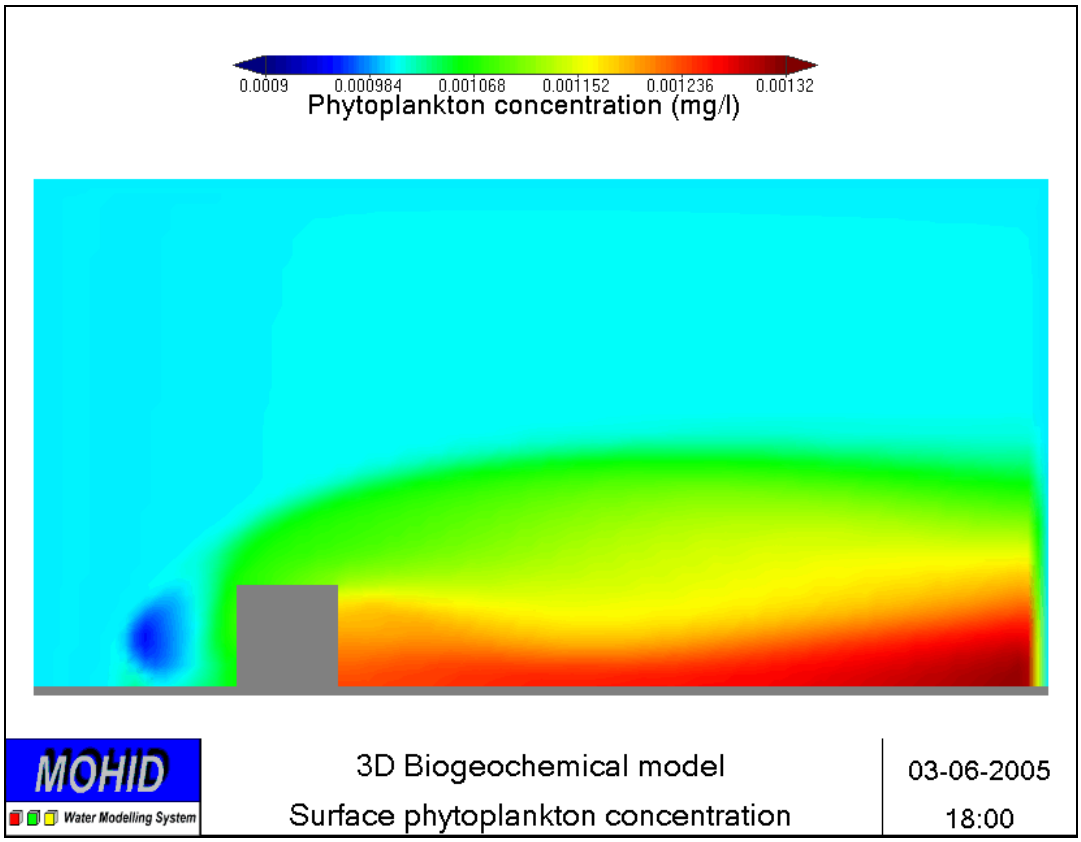

Figure 31 - Surface phytoplankton concentration after 2 days and 6 hours of simulation

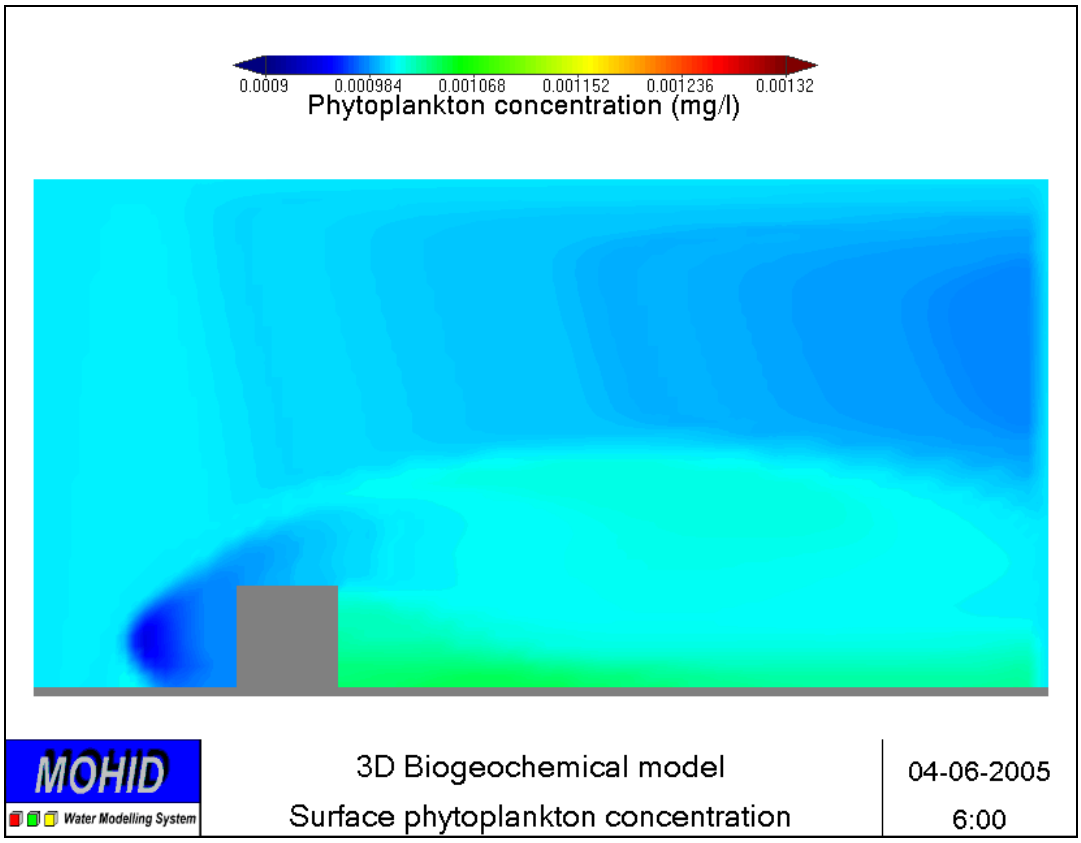

Figure 32 - Surface phytoplankton concentration after 2 days and 18 hours of simulation

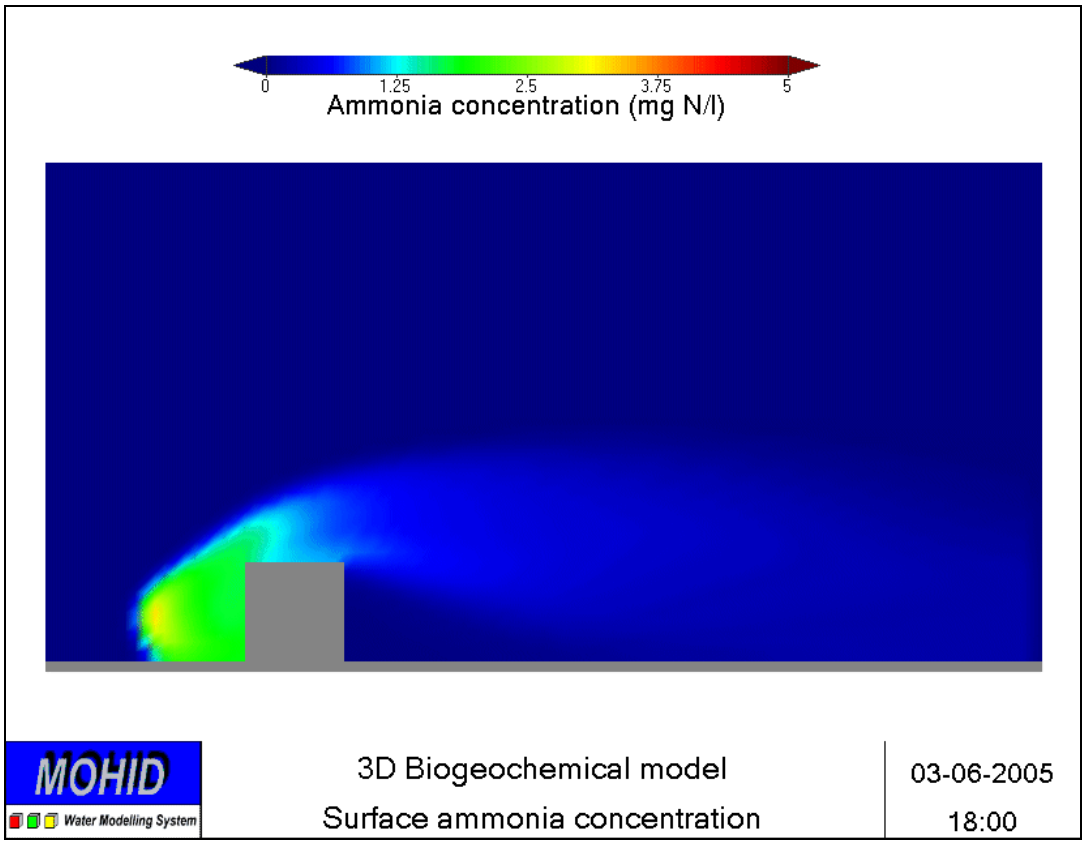

Figure 33 - Surface ammonia concentration after 2 days and 6 hours of simulation

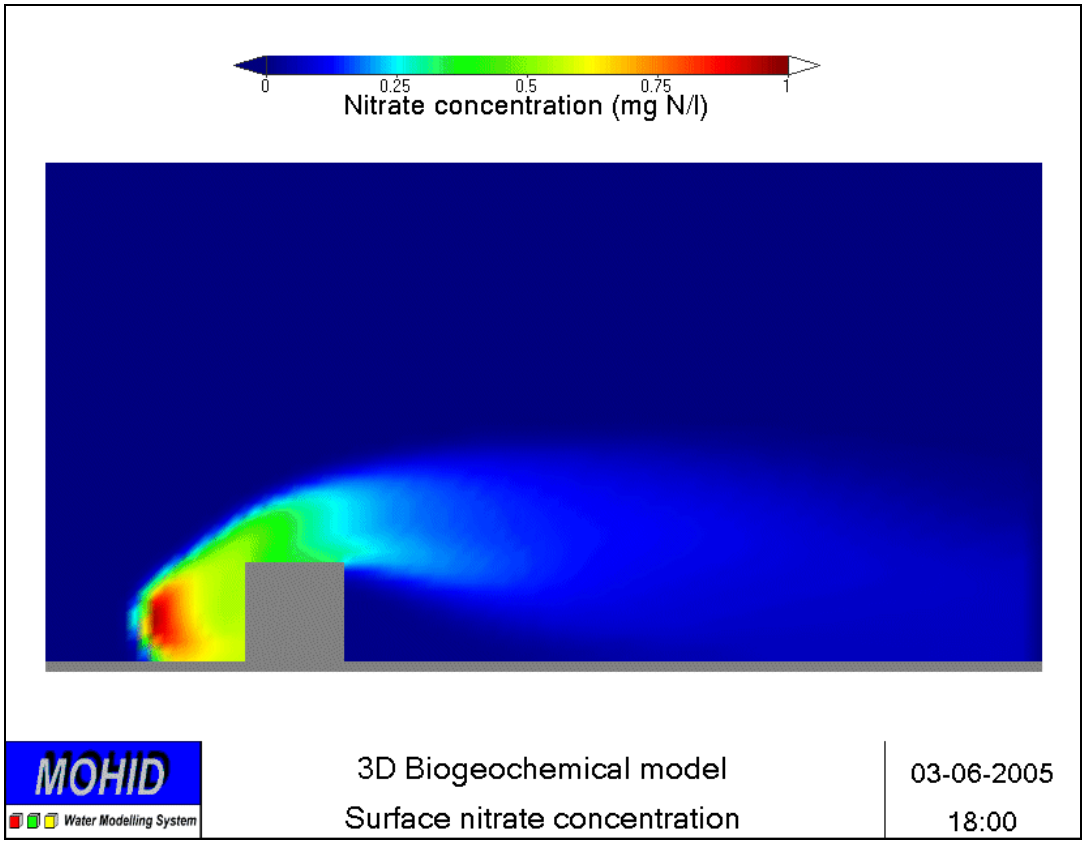

Figure 34 - Surface nitrate concentration after 2 days and 6 hours of simulation

6.1.2 About the Runs

The simulation was done in a PC running on Microsoft Windows XP Professional, equipped with a 3.4 Ghz Intel Pentium IV Processor and required 70MB RAM. The run took around 9 hours of CPU time. The model was compiled with Intel FORTRAN Compiler 9.0. The time required for implementing the test case and preparing the figures was about 1 day*person.

7. Conclusions

The results of the hydrodynamic model have shown that the solution is highly dependent on the boundary condition used putting into evidence that on one hand (1) it is very important to specify exactly the conditions of the simulation (as was done in the questionnaire), and on the other hand (2) for real situations it is important to have a model able to use the most adequate boundary conditions.

Using the boundary conditions specified in the questionnaire, the flow is controlled by inertia and converges to the southern corner next to the eastern boundary. Behind the obstacle there is a region of low velocity, but no recirculation is identified. Using a cyclic/radiative boundary condition, emulating an infinite rectilinear coastline where an obstacle is placed, velocities are higher and the general flow is controlled by longitudinal equilibrium between wind drag and bottom friction and transversally by equilibrium between Coriolis and pressure forces.

The results of the 3D simulations put into evidence the importance of the vertical processes in flows where density plumes are submitted to a surface wind forcing. In the case studied, surface velocity increased by about 25% and the recycling zone in the shadow of the obstacle does not reach the surface (because the wind is very strong).

The biogeochemical processes are not very important in this case because the residence time is of the order of 6 hours. The results showed however that they are more important in the shallower areas and in regions downstream the modelling area.

The Lagrangian simulations are not very useful in this particular case because the plume dimension is of the order of the size of the simulation domain (one half). They would however be very useful in real situations when the area of simulation must be much larger than the plume size (because of wind direction variability and for simulating the fate of the material discharged and not only the dispersion in the vicinity of the diffuser).

For obtaining results quickly and for simplifying code maintenance/expansion the model, likewise MOHID, must (1) have a well organized and clear code, (2) deal with boundary conditions on a systematic way, (3) have a robust input module (for avoiding input data errors) and (4) be equipped with a good post processing tool. Thus, the sum of pre-processing, execution and post-processing times is less important then the time occupied in scenarios definition and results analysis and interpretation, when the aim is to produce high quality simulations.

8. References

Burchard, H. & K. Bolding (2001). Comparative Analysis of four second-moment turbulence closure models for the Oceanic Mixed Layer. Journal of Physical Oceanography 31, 1943-1968.

Canuto, V.M., A. Howard, Y, Cheng e M.S. Dubovikov (2001): Ocean Turbulence. Part I: One-Point closure model momentum and heat vertical diffusivities, Journal of Physical Oceanography 31, 1413-1426.

Chapman, D. C., 1985. Numerical treatment of cross-shelf open boundaries in a barotropic coastal ocean model, J. Phys. Oceanogr., 25, 1060-1075, 1985.

EPA, 1985, Rates, constants and kinetics formulations in surface water quality modelling (2nd edition), United States Environmental Protection Agency, Report EPA/600/3-85/040, 454 pp.

Flather, R.A., 1976: A tidal model of the northwest European continental shelf. Mem. Soc. R. Sci. Liege, Ser. 6(10), 141-164.

Leitão (2003). Integração de Escalas e de Processos na Modelação no Ambiente Marinho, PhD thesis, IST, Technical University of Lisbon, Portugal.

Palma, E. D. and R. P. Matano, 1998: On the implementation of passive open boundary conditions for a general ciruclation model: The barotropic mode, Journal of Geophysical Research, 103, 1319-1342 (1998).

Pina, P., 2001, An integrated approach to study the Tagus estuary water quality; Master Dissertation in Marine resources ecology, management and modelling, Instituto Superior Técnico, Technical University of Lisbon, Portugal, 70 pp.